Formation evaluation using conventional and special core analyses: Belayim Formation as a case study, Gulf of Suez, Egypt

Bassem S. Nabawy[1] · **Moataz Kh. Barakat**[2]

Abstract The present study aims to throw the light on the importance of the conventional and special core analyses in the integration with the petrographical studies for the formation evaluation of the reservoir rocks. The petrographical studies include the microfacies analysis and studying the diagenetic factors that predominated during the diagenetic history of the Belayim rock sequence in the study area. Two zones of Belayim Formation in the onshore Belayim oil field (the upper level (zone IIA) represents Hammam Faraun member and the lower one (zone IV) represents Sidri member) were studied. The measured routine core analyses data includes porosity (helium and summation fluids), density (grain and bulk), permeability (horizontal and vertical) and fluid saturations (oil and water). In addition, the formation resistivity factor, irreducible water saturation, Archie's parameters (*a*, *m* and *n*), liquid permeability, relative permeability, wettability, the pore throat distribution, as well as the porosity and permeability measured under high pressure were measured as a special core analyses procedure. From the integration of the aforementioned petrographical and petrophysical studies, the Belayim Formation can be discriminated into three petrophysical facies (Facies-1, Facies-2 and Facies-3) described petrographically as (1) Facies-1 (argillaceous subfeldspathic arenite microfacies), (2) Facies-2 (siliceous quartz arenite microfacies) and (3) Facies-3 (dolomitic sublithic arenite microfacies). The petrophysical Facies-2 (siliceous microfacies) is characterized by the best reservoir properties (rank III, very good average porosity, very good permeability, fair to very good reservoir quality index (RQI) and relatively poor to good flow zone indicator (FZI), neutral to moderately oil wet and more than 75% macropores and mesopores). On the other side, samples of the petrophysical Facies-1 (argillaceous microfacies) have the lowest reservoir potential (rank VI, poor average porosity, poor to fair permeability, poor to impervious RQI and relatively poor to fair FZI and more than 50% micropores and nanopores). Therefore, it is recommended to use the conventional and special core analyses data in the integration with the petrographical studies as a good procedure for the formation evaluation and discrimination of the reservoir sequence into different flow units.

This article is part of the Topical Collection on *Current Advances in Geology of North Africa*

✉ Bassem S. Nabawy
bsnabawy@yahoo.co.uk

Moataz Kh. Barakat
moatazbarakat@yahoo.com

[1] Department of Geophysical Sciences, National Research Centre, Cairo, Egypt

[2] Department of Geology, Faculty of Science, Tanta University, Tanta, Egypt

Introduction

During the Late Oligocene–Early Miocene, the African rift system rejuvenated and the eastern part of the African plate has been broken into the Arabian, Nubian and Sinai plates (Jarrige et al. 1990; Bosworth et al. 1998; Montenat et al. 1998). During that time, the Lower Miocene deposits accumulated forming a good sequence of source rocks, while the subsequent continuous deposition of the Middle Miocene sandstones and Upper Miocene evaporites formed the main

reservoir and seal rocks in the Gulf of Suez. The Middle Miocene sequence in the Gulf of Suez is considered as a syn-rift megasequence that can be differentiated into four formations; from top to bottom, they are Belayim, Kareem, Rudies and Nukhul formations. These formations are topped by the Upper Miocene evaporites of South Gharib, Zeit and post-Zeit formations. Belayim Formation, the target of the present study, forms the top of the Middle Miocene sequence and consists of two clastic members (Hammam Faraun and Sidri members) alternated with two evaporate members (Feiran and Baba members). Its geological and structural setting as well as its hydrocarbon potential were studied by many authors (e.g. EGPC 1964; El-Gezeery and Marzouk 1974; Scott and Govean 1985; Gawad et al. 1986; Meshref et al. 1988; Rashed 1990; Hughes et al. 1992; AlSharhan and Salah 1994; Ramzy et al. 1996; Ramadan and Eysa 2012; Nabawy and El Sharawy 2015; El-Khadragy et al. 2016; etc.).

The main target of the present study is to evaluate the hydrocarbon potential of the Belayim Formation in its onshore oil field in Egypt (well BB-4, Fig. 1) using the conventional and special core analyses data. The conventional core analyses are usually used to calibrate the well log data based on the measured porosity (in volume fraction) and permeability (in md). In addition, Amaefule et al. (1993) used the routine core analyses data, including porosity and permeability, for discriminating the reservoir rocks into different zones based on their quality. This technique is called the reservoir discrimination technique, which is based on both the reservoir quality index (RQI) and the flow zone indicator (FZI), that has been successfully examined and applied by many authors (e.g. Tiab and Donaldson 1996; Al-Dhafeeri and Nasr-El-Din 2007; Othman et al. 2008; Kassab et al. 2015; etc.). More recently, the concept of the 'RQI' was applied supported by the new concept of the reservoir potential index (RPI) that was proposed to introduce more precise characterization for the reservoir quality and discrimination into flow zones of different ranks.

Fig. 1 Location map of the studied Belayim Formation, well BB-4, onshore Belayim oil field, Gulf of Suez, Egypt

On the other side, the special core analyses can be used as a supporting technique for the routine core analyses in the formation evaluation and the reservoir discrimination.

The electric resistivity measurements, as a special core analyses procedure, are a good tool for defining in precise the actual values of the saturation exponent 'n', porosity exponent 'm' and the lithology factor 'a' (Archie 1942). These parameters have a great importance in estimating the hydrocarbon reserves, where a small shift in their values will cause a great shift in estimating the reserves (Nabawy 2015).

In addition, the mercury injection technique can introduce a full and precise characterization for the pore throat distribution that supports the reservoir discrimination into zones of different ranks (Nabawy et al. 2009a). On the other side, the relative permeability and wettability are measures for the interactive relationship between the hydrocarbons and the bearing rocks, where they indicate the nature of the reservoir rocks as an oil or water wet, i.e. they are a direct indication for the ease by which the oil can be withdrawn and the for future estimation for the reservoir performance.

Consequently, the present research introduces the conventional and special core analyses as precise tools for evaluating the potential ranks of the reservoir rocks and their discrimination into productive, super productive and non-productive zones.

Methods and techniques

To study the mineral composition and the diagenetic history of the studied Belayim samples as well as their texture and structure, a number of thin sections (representative for two studied oil prospective zones: zone IIA of Hammam Faraun member at depth interval 2485–2504 m and zone IV of Sidri member at depth interval 2600–2618 m) were prepared for the petrographical studies under the polarized microscope. The studied microfacies and pore types were classified and discriminated using the sandstone's classification of Pettijohn et al. (1972) and following the pore type nomenclature of Choquette and Pray (1970).

For studying the grain-to-grain (petrofabric) and the pore-to-pore (pore fabric) relationships of the studied samples, another set of samples, representing the different facies, were studied using the scanning electron microscope (SEM). In addition, to reveal the mineral composition, a number of additional samples were examined using the X-ray diffraction (XRD) technique.

For the routine core analyses, a total number of 120 cleaned and dried plug samples were studied petrophysically by measuring the bulk and grain densities 'σ_b and σ_g', the helium and summation fluid porosity '$\varnothing_{He}$ and $\varnothing_{SF}$', the gas permeability in the horizontal and vertical directions 'k_H and k_V' as well as by measuring the water 'Sw' and oil saturation 'So' (for fresh non-cleaned samples).

Porosity and permeability of the studied samples were ranked following the reservoir rank classification of Levorsen (1967) that was modified by Nabawy et al. (2009b) and Nabawy (2015).

Anisotropy of permeability 'λ_k' was calculated (following Serra 1988; Nabawy and El-Hariri 2008; Nabawy 2015; etc.…) as follows.

$$\lambda_k = \left(k_{max} \Big/ k_{min} \right)^2 \tag{1}$$

Processing the routine core analyses data was followed by discriminating the studied reservoir rocks into flow units using the RQI and the FZI of Amaefule et al. (1993) as well as calculating the rank of the RPI as follows.

$$RQI = 0.0314 \sqrt{\frac{k}{\varnothing}} \tag{2}$$

$$FZI = \frac{RQI}{NPI} = \frac{0.0314\sqrt{k/\varnothing}}{\varnothing \Big/ (1-\varnothing)} \tag{3}$$

where, NPI is the normalized porosity value.

$$RPI = \frac{RQI + FZI}{2} \tag{4}$$

The special core analyses measurements, including the formation resistivity (FR) factor, the relative permeability, the pore throat distribution and the wettability as well as the effect of overburden pressure on the petrophysical properties, have been applied for a total of 84 cleaned and dried plugs.

The apparent electric resistivity 'Ro' was measured at ambient conditions and fixed electric frequency (1 kHz) for plugs saturated by 237 kppm (Rw = 0.0593 Ω m) saline solution for plugs from zone IIA and 295 kppm (Rw = 0.0545 Ω m) for plugs from zone IV. The FR factor was then determined by dividing the 'Ro' for each plug on the electric resistivity of its saturating saline 'Rw'.

$$FR = Ro \Big/ Rw \tag{5}$$

For studying the effect of overburden pressure on porosity (porosity reduction (PR)) and the FR factor, the Ro of the studied samples was measured once more at gradually increased high confining pressure (at 400, 1000, 1500, 2000, 3000, 4000, 5000 and 6000 psi). Then, the resistivity index (RI) was measured for each plug sample by measuring the electric resistivity at different brine saturations by desaturating the fully brine-saturated samples using the centrifuge, where the measured resistivity 'Rt' at each brine saturation percentage was divided by its resistivity at 100% full brine saturation 'Ro' as follows.

$$RI = Rt\big/Ro \qquad (6)$$

In addition, the saturation exponent 'n' was determined by plotting the 'RI' versus the saline saturation percentage Sw as follows.

$$Sw^n = 1\big/RI \qquad (7)$$

The wettability was measured using Amott method, where the Amott wettability index (Amott relative displacement index (AI)) was calculated as the difference between the wettability index of the rock to the water and the oil. It is indicated by a value that varies between 0 and ±1; the negative value refers to oil wet reservoir, whereas the positive values indicate a water wet reservoir. For the present study, the measured wettability was ranked following a proposed classification as shown in Table 1.

For studying the relative permeability, the plugs were measured using a water saline-oil flushing system, whereas the pore throat distribution was studied by using the mercury injection capillary pressure (MICP) technique at incremental confining pressure up to 2000 psi. The studied reservoir sequence was then discriminated into different ranks based on the pore throat distribution as shown in Table 2. Results of the measured routine and special core parameters were introduced in Tables 3, 4, 5, 6 and 7.

Lithostratigraphy

The Middle Miocene Belayim Formation (Middle to Upper Serravallian) in the Gulf of Suez has a great importance, due to its role as one of the most prolific reservoir rocks and as a seal rock. It underlies the South Gharib evaporates and unconformably overlies the Kareem Formation (Fig. 2). It was deposited in shallow marine to lagoonal environments with a good thickness and widespread occurrences in the Gulf of Suez, particularly in the central and southern provinces. It is composed of four members; from top to bottom, they are

Table 1 A proposed classification for ranking the wettability of the studied samples based on the Amott index data

Wettability rank	Amott index (AI)
Strongly water wet	$0.8 < AI \leq 1.0$
Moderately water wet	$0.6 < AI \leq 0.8$
Weakly water wet	$0.3 < AI \leq 0.6$
Neutral	$-0.3 < AI \leq 0.3$
Weakly oil wet	$-0.6 < AI \leq -0.3$
Moderately oil wet	$-0.8 < AI \leq -0.6$
Strongly oil wet	$-1.0 < AI \leq -0.8$

Hammam Faraun, Feiran, Sidri and Baba members. These members are deposited in consequence with three unconformities separating each one from the other. The lithology of the studied Belayim Formation in well BB-4 can be described as 290 m of intercalations of sandstones, shales and evaporites.

1. Hammam Faraun member (104 m): It is composed of 41-m shales intercalated with some sandstone interbeds at the top of the member followed downward by 49.0 m of anhydrite and 14.0 m (zone IIA) of sandstones deposited in tidal flat to intertidal environments (represents a phase of sea transgression) causing increase of the sand content towards the margins of the basin (Nabawy and El Sharawy 2015).

2. Feiran member (82.0 m): It is composed of anhydrite intercalated with few streaks of shales deposited in shallow marine to lagoon conditions (represents a phase of sea regression).

3. Sidri member (49.0 m): It is composed of partially dolomitized sandstones intercalated with shale streaks (zone IV) and deposited in inner neritic to littoral marine environment (represents a second phase of sea transgression). It is considered as the thinnest member of the Belayim Formation (Nabawy and El Sharawy 2015).

4. The Baba member (55.0 m): It is composed of anhydrite with some shale interbeds deposited in shallow marine to lagoon conditions (represents a second phase of sea regression).

The lithostratigraphic column of the Belayim Formation in the studied area and its cored parts (zones IIA and IV) are shown in Fig. 2.

Petrographical studies

Microfacies analysis

The studied Belayim sandstone samples can be subdivided into three microfacies association; namely, they are argillaceous subfeldspathic arenite, siliceous quartz arenite and dolomitic sublithic arenite microfacies.

Argillaceous subfeldspathic arenite microfacies

It is representative for the lowest parts of zone IV of Sidri member. It is composed of ill sorted, very fine to moderate quartz grains and unaltered to highly altered feldspars (up to 18.3%) represented by microcline and orthoclase (Fig. 3a) as well as some fine glauconite pellets, phosphatic remains and rounded rock fragments composed of basement rocks and sandstones surrounded by iron oxide rims. The phenoclasts

Table 2 A proposed classification based on the pore diameter 'D' distribution obtained from the mercury injection capillary pressure (MICP) technique

Pore diameter	Megapores $D \geq 100$ μm	Macropores $100 > D \geq 10$ μm	Mesopores $10 > D \geq 1.0$ μm	Micropores $1.0 > D \geq 0.01$ μm	Nanopores 0.01 μm $> D$
Rank I	$P \geq 25.0\%$	$P \geq 50.0\%$		$P < 25.0\%$	
Rank II	$P < 25.0\%$	$P \geq 50.0\%$		$P < 25.0\%$	
Rank III	0.00	$P \geq 75.0\%$		$P < 25.0\%$	
Rank IV	0.00	$P < 75.0\%$		$P \geq 25.0\%$	
Rank V	0.00	0.00	$P \geq 50.0\%$	$P < 50.0\%$	
Rank VI	0.00	0.00	$P < 50.0\%$	$P \geq 50.0\%$	

are cemented together by ferruginated clay patches and iron oxides with some silica cement which greatly reduced the interstitial pore spaces (Fig. 3a). The presence of extraordinary fracture system in some quartz and feldspar grains slightly increased porosity of few samples (Fig. 3b). Alteration of feldspars into kaolinite booklets sometimes closed the interconnected pore system of the studied samples (Fig. 3c).

Porosity is mostly negligible to poor (less than 10%), sometimes fair (10–15%). It is represented by (1) intergranular porosity, mostly reduced by clay patches and iron oxides (Fig. 3c), (2) microfracture porosity, due to fractured grains and (3) matrix porosity in the clay patches.

Siliceous quartz arenite microfacies

Most parts of the cored interval of the Hammam Faraun member and few parts of Sidri member are represented by the present microfacies which is composed of ill sorted, fine to medium, rounded to angular quartz grains cemented together by silica cement which slightly reduced the pore spaces (Fig. 3d) and rarely blocked some channels (Fig. 3e). The quartz grains (monocrystalline and rarely polycrystalline) are compacted together through suture and concave-convex contact with slight effect on the total pore volume where the grains are mostly floating within the cement.

Few highly altered feldspar grains, ferruginated clay patches, glauconite pellets and lithic fragments are present. Porosity of the siliceous quartz arenite samples is mostly very good to excellent ($\geq$20%) and represented mostly by (1) intergranular pore spaces and (2) microfractures, due to some stress acted on the present grains.

Dolomitic sublithic arenite microfacies

This microfacies represents the top most parts of 'zone IV' of Sidri member and the lowest parts of 'zone IIA' of Hammam Faraun member. It is composed of ill sorted, very fine to coarse quartz grains, beside to some lithic fragments composed of limestone, sandstone, claystone and rarely of schist ($\leq$15.6%), as well as feldspars ($\leq$8.56%), glauconite pellets ($\leq$6.06%) and bioclastic remains ($\leq$5.05%). The phenoclasts

are cemented together by dolomitic cement represented mostly by euhedral, tiny to fine dolomitic rhombs ($\leq$26%) which are interlocked together due to upgrading neomorphism. In addition to the dolomitic, some ferruginated clay patches and rare calcite relics are present.

The present microfacies is mostly characterized by poor to good porosity values (5–15%), described as (1) microintergranular pores, moderately to highly reduced by euhedral dolomite rhombs, sometimes are blocked (Fig. 3f); (2) fracture porosity in fractured grains; (3) intercrystalline porosity and (4) matrix porosity.

Impacts of diagenetic factors on the pore volume

The diagenetic processes have a great effect on the petrophysical properties of the porous rocks by reducing or enhancing the pore volume and pore connectivity. They can be classified based on their effect on the pore volume into factors that reduce porosity (e.g. compaction, cementation, aggrading neomorphism, formation of authigenic minerals as well as initial and late stages of dolomitization) and other that enhance porosity (e.g. dissolution and leaching out, middle stage of dolomitization and fracturing).

Porosity-reducing diagenetic factors

Cementation Cementation is the most important porosity-reducing diagenetic processes. For the siliceous quartz arenite microfacies, silica cement is the main cement which slightly reduced the intergranular porosity. It is mostly represented by meniscus 'gravity' cement and pressure solution due to the grain-to-grain compaction. Sometimes, the silica cement is responsible for closing the pore channels (Fig. 3e). The effect of the silica cement is accompanied and supported by the reducing effect of the clay patches for the argillaceous subfeldspathic arenite and dolomitic sublithic arenite microfacies. Therefore, its final effect is greater for these two microfacies.

The calcite cement is rarely present (Fig. 3d, e) and mostly obliterated due to the diagenetic dolomitization process. It is represented by micrite patches filling the pore spaces and precipitated on the grain surfaces as well as micro to pseudo

Table 3 Values of the petrophysical parameters of the Belayim samples obtained from the routine core analyses

Facies no.	Microfacies composition	Number		σ_b (g/cm³)	σ_g (g/cm³)	$\varnothing_{He}$ (%)	$\varnothing_{SF}$ (%)	k_H (md)	k_V (md)	λ_k (0.00)	So (%)	Sw (%)	RQI (μm)	FZI (μm)
Facies-1	Argillaceous subfeldspathic arenite	28 Plugs	Mean	2.48	2.66	6.47	7.38	5.84	3.02	1.85	4.27	69.4	0.23	3.40
			Min.	2.32	2.59	2.20	1.58	0.35	0.10	1.08	0.00	16.8	0.09	1.40
			Max.	2.62	2.68	11.8	15.5	51.1	32.7	3.89	26.4	96.3	0.68	6.59
Facies-2	Siliceous quartz arenite	48 Plugs	Mean	2.10	2.67	21.3	18.5	231.7	215.4	1.12	18.4	47.5	0.81	2.81
			Min.	1.98	2.64	14.7	14.7	6.28	5.60	0.66	5.35	28.9	0.18	0.82
			Max.	2.29	2.68	25.8	22.9	1197	1159	2.10	31.2	59.7	2.15	6.28
Facies-3	Dolomitic sublithic arenite	43 Plugs	Mean	2.37	2.71	12.7	11.1	43.3	30.6	1.15	11.7	54.3	0.43	2.80
			Min.	2.09	2.69	5.20	3.29	0.63	0.62	0.70	0.00	27.4	0.10	1.34
			Max.	2.60	2.79	22.2	21.0	350.7	156.0	1.94	38.0	91.9	1.25	4.50

σ_b bulk density, σ_g grain density, $\varnothing_{He}$ helium porosity, $\varnothing_{SF}$ summation fluids porosity, k_H horizontal permeability, k_V vertical permeability, So oil saturation, Sw water saturation, RQI reservoir quality index, FZI flow zone indicator, λ_k anisotropy of permeability

Table 4 The special core analyses data at the ambient pressure (14.5 psi) and at the confining pressure (6200 psi) for the studied Belayim samples

Facies no.	Microfacies composition	Number		FR (0.00) at 14.5 psi	$\varnothing_{He}$ (%)	m (0.00)	FR (0.00) at 6200 psi	$\varnothing_{He}$ (%)	m (0.00)	RI (0.00)	Sw_{irr} (%)	n (0.00)
Facies-2	Siliceous quartz arenite	8 Plugs	Mean	14.1	20.8	1.64	20.1	18.6	1.69	18.7	26.3	2.18
			Min.	9.2	14.7	1.62	12.4	12.4	1.59	11.2	22.4	2.10
			Max.	22.6	25.8	1.68	35.6	23.3	1.80	29.6	31.7	2.29
				$FR = \dfrac{1.09}{\phi^{1.58}} = \dfrac{1}{\phi^{1.64}}$			$FR = \dfrac{1.43}{\phi^{1.52}} = \dfrac{1}{\phi^{1.69}}$			$RI = \dfrac{0.81}{Sw_{irr}^{2.29}}$		
Facies-3	Dolomitic sublithic arenite	6 Plugs	Mean	38.8	10.8	1.56	20.1	18.6	1.73	10.6	29.8	1.95
			Min.	18.0	5.1	1.44	12.4	12.4	1.67	8.0	26.1	1.82
			Max.	72.7	16.4	1.64	35.6	23.3	1.88	13.9	34.7	1.99
				$FR = \dfrac{2.47}{\phi^{1.14}} = \dfrac{1}{\phi^{1.56}}$			$FR = \dfrac{2.79}{\phi^{1.24}} = \dfrac{1}{\phi^{1.73}}$			$RI = \dfrac{1.00}{Sw_{irr}^{1.92}}$		

FR formation resistivity factor, $\varnothing_{He}$ helium porosity, m porosity exponent, RI resistivity index, Sw_{irr} irreducible water saturation, n cementation exponent

Table 5 The gas and liquid permeability average values 'k_G and k_L', porosity '$\varnothing$', the permeability values contributed by the micropores and nanopores 'k_μ' for the studied samples and the effect of confining pressure on porosity indicated by the porosity reduction (PR) index

Facies no.	Microfacies composition	Number		k_G (md)	k_L (md)	k_μ (%)	$\varnothing$ (%)	Helium porosity, $\varnothing_{He}$ (%)							PR (%)
								400 psi	1000 psi	1500 psi	2000 psi	3000 psi	4000 psi	6000 psi	
Facies-2	Siliceous quartz arenite	10 Plugs	Mean	380.2	288	43.1	20.9	22.9	22.1	21.7	21.5	21.1	20.9	20.6	10.1
			Min.	10.5	5.1	12.0	6.3	19.2	18.8	18.6	18.4	18.3	18.2	18.0	5.9
			Max.	1242	1093	80.3	42.7	25.5	25.1	24.8	24.6	24.4	24.2	24.0	14.9
Facies-3	Dolomitic sublithic arenite	8 Plugs	Mean	84.6	40.9	54.1	18.2	13.0	12.8	12.6	12.5	12.4	12.3	12.2	6.2
			Min.	3.33	1.11	36.9	9.5	6.1	6.0	5.9	5.8	5.7	5.7	5.5	4.0
			Max.	206	108	83.0	22.9	19.6	19.3	19.2	19.1	19.0	18.9	18.8	9.8

sparite patches cemented the phenocrysts together and filling the pore spaces.

Compaction Compaction due to increasing the stress effect on the studied sandstone samples caused different grades of strained grains which are compacted together in a suture, concave-convex and straight contacts (Fig. 3d, e). Sometimes, compaction led to creating subordinary fracture system through fracturing the brittle quartz grains (Fig. 3b). However, the porosity-reducing effect of the compaction compensated the porosity-enhancing effect of the dissolution and leaching out of the fractured grains.

Authigenic minerals The authigenic minerals are among the most important factors that reduce the pore volume and the pore connectivity in particular. Kaolinite is the most common authigenic clay mineral in sedimentary rocks. The kaolinite is the most common authigenic mineral which was formed due to alteration of the feldspar grains, particularly for the argillaceous subfeldspathic arenite microfacies. The authigenic stacked kaolinite booklets are present as a filling material for the pore spaces and as a blocking material for reducing the pore connectivity (Fig. 3c). Some pyrite and iron oxides are attached to the quartz grain surfaces and mixed with the clay patches of the argillaceous subfeldspathic microfacies.

Porosity-enhancing diagenetic factors

Fracturing Fracturing is usually related to increasing stresses acting beyond the elastic stage of a brittle material, e.g. the brittle quartz grains which are characterized by limited elastic stage. It is usually formed due to tensional forces which increase the pore volume via creating an extra fracture pore system, e.g. the microfracture system that created through the quartz grains of the argillaceous subfeldspathic arenite microfacies (Fig. 3b). The presence of more than one direction of these microfractures helps in creating a connected pore system with a high grade of connectivity, i.e. it increases the ability of solutions to invade, to dissolve and to leach out the dissolved rock mass.

Dissolution and leaching out During the post diagenetic history of sandstones, the primary intergranular porosity is mostly reduced due to later cementation which is mostly compensated by dissolution and leaching out of the rock mass as a porosity-enhancing diagenetic factor. For the present samples, dissolution is indicated by the presence of some altered to highly altered feldspars as well as the presence of some authigenic kaolinite content. Leaching out of the dissolved material is a critical process for enhancing porosity (Fig. 3a); otherwise, many clay patches are formed to decrease the total pore volume, e.g. the argillaceous subfeldspathic arenite microfacies (Fig. 3b).

Table 6   Wettability data using Amott index technique for the studied samples

Facies no.	Microfacies composition	Number	Depth	k_G (md)	$\varnothing$ (%)	Sw_{irr} (%)	So_r (%)	Amott index	Wettability
Facies-2	Siliceous quartz arenite	7 Plugs	2604.73	902	24.7	17.0	26.5	−0.550	Weak oil wet
			2491.86	79.0	20.2	27.4	43.2	−0.641	Moderately oil wet
			2605.43	570	23.6	12.5	38.0	−0.762	Moderately oil wet
			2492.04	63.0	22.3	22.6	37.4	−0.619	Moderately oil wet
			2604.07	664	25.3	22.1	33.7	0.283	Neutral
			2609.85	352	18.2	37.5	21.5	0.299	Neutral
			2489.67	62.8	16.4	42.2	14.0	0.308	Weak water wet
Facies-3	Dolomitic sublithic arenite	5 Plugs	2488.77	37.0	19.1	19.1	27.5	−0.485	Weak oil wet
			2613.05	44.0	16.0	25.2	30.5	−0.505	Weak oil wet
			2614.16	462	25.6	13.5	43.2	−0.920	Strongly oil wet
			2488.42	4.77	14.9	17.2	36.0	−0.448	Weak oil wet
			2488.17	0.04	6.5	69.0	23.3	0.500	Weak water wet

k_G gas permeability, $\varnothing$ measured porosity, Sw_{irr} irreducible water saturation, So_r residual oil saturation

Porosity-enhancing/reducing diagenetic processes

The dolomitization process can be classified into three stages: initial stage (pore-filling phase), middle stage (selective dolomitization phase) and late stage (neomorphism phase). He added that the effect of dolomitization on porosity, whether it is reducing or enhancing effect, is based on the progress of the dolomitization phase. The initial and late stages of dolomitization have a reducing effect on the pore volume and connectivity, whereas the middle stage of dolomitization is considered as an enhancing pore volume process.

Table 7   Different petrophysical parameters of the studied samples and their mercury porosity parameters obtained from the mercury injection capillary pressure (MICP) technique

Facies no.	Microfacies composition	Number	k_G (md)	$\varnothing_{Hg}$ (%)	Threshold pressure (psi)	Macropores	Mesopores	Micropores	Rank
Facies-1	Argillaceous subfeldspathic arenite	4 Plugs	2.97	8.0	150	0.00	15.8	84.2	VI
			14.7	11.4	40.0	0.00	71.6	28.4	V
			1.63	5.6	40.0	0.00	49.6	51.4	VI
			0.41	5.7	80.0	0.00	45.8	54.2	VI
		Mean	4.9	7.68	77.5	0.00	45.7	54.5	VI
Facies-2	Siliceous quartz arenite	9 Plugs	8.7	21.7	15.0	24.8	49.4	25.8	IV
			9.8	25.4	12.0	24.6	48.6	26.8	IV
			21.0	16.4	15.0	8.50	66.6	24.9	IV
			48.8	18.2	12.0	16.3	58.2	25.5	IV
			403	27.0	9.0	42.1	37.4	20.5	IV
			167	23.7	9.0	28.5	46.9	24.6	IV
			856	24.2	9.0	50.1	39.2	10.7	III
			588	24.0	5.0	67.6	19.4	13.0	III
			20.3	12.6	24.0	3.60	70.4	26.0	IV
		Mean	236	21.6	12.2	29.6	48.4	22.0	III
Facies-3	Dolomitic sublithic arenite	4 Plugs	69.7	22.1	12.0	36.5	40.4	23.1	III
			104	18.6	10.2	39.5	42.0	18.5	III
			5.0	10.6	21.0	1.30	55.9	42.8	IV
			38.7	18.4	18.0	16.4	52.6	31.0	IV
		Mean	54.4	17.4	15.3	23.4	47.7	28.9	IV

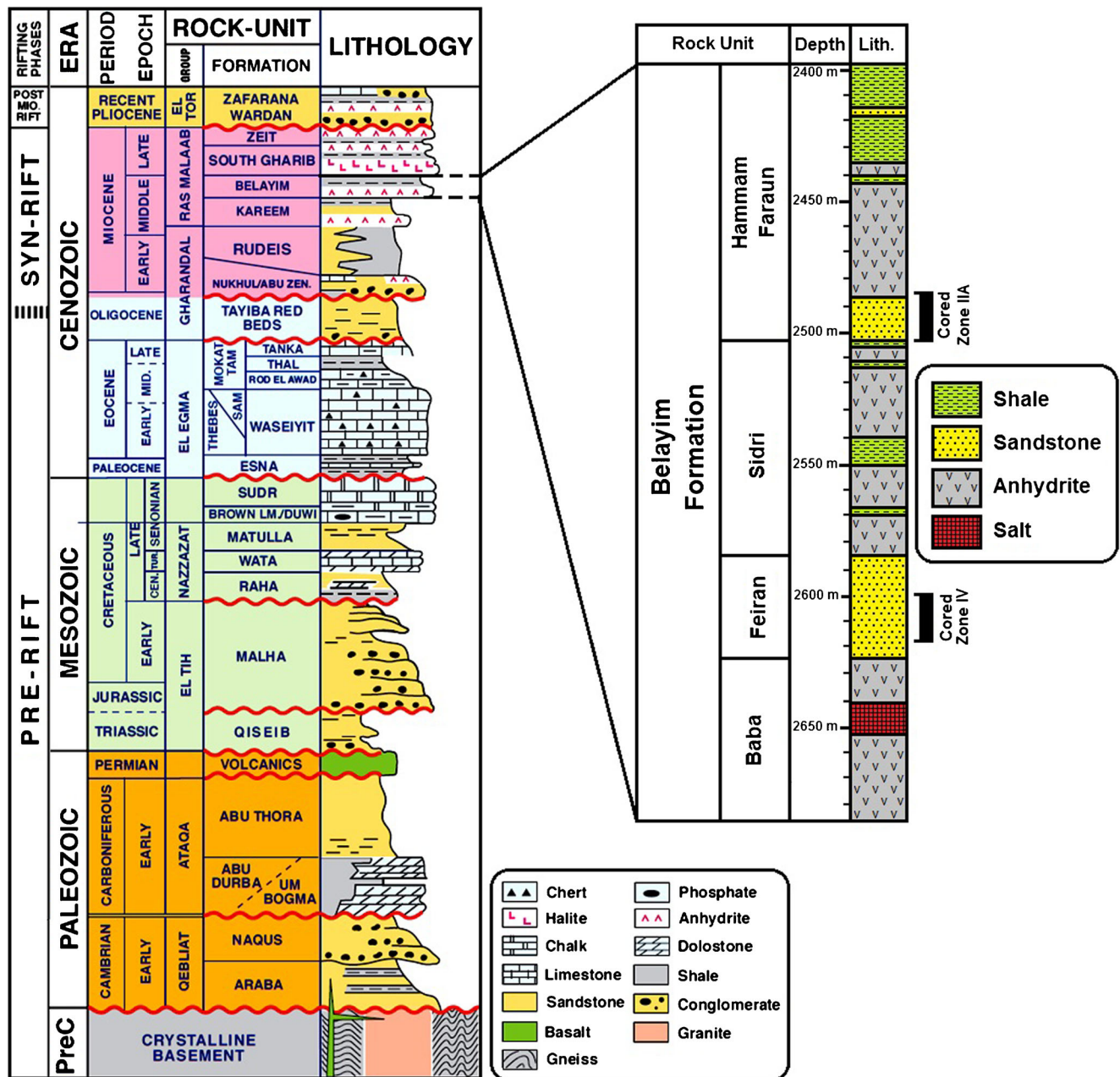k_G gas permeability, $\varnothing_{Hg}$ measured porosity using MICP technique

Fig. 2 A generalized stratigraphic column for the sedimentary rocks on the eastern shore of the Gulf of Suez, Egypt, with emphasis on the lithostratigraphy of Belayim Formation (modified after Darwish and El-Araby 1993)

Middle stage of dolomitization (porosity-enhancing factor) As mentioned before, dolomitization in its middle stage 'selective dolomitization stage' is responsible for enhancing porosity. For the present study, the selective dolomitization is one of the main porosity-enhancing factors as in the case of the dolomitic sublithic arenite microfacies.

Initial and late stages of dolomitization (porosity-reducing factor) For dolomitic sublithic arenite microfacies, dolomitization is represented by euhedral to idiotopic and drusy dolomite rhomb occluded porosity that was created during the middle stage of dolomitization 'volume replacement phase' which caused enhancement of porosity due to the selective dolomitization. It seems that the dolomitization process of the present samples is in midway transitional stage between the middle stage of dolomitization 'porosity-enhancing' and its last stage 'porosity-reducing'. So, the reducing effect of dolomitization is slight but sometimes is highly effective due to filling and blocking the interstitial pore spaces (Fig. 3f). The studied dolomite rhombs are mostly characterized by zonation and cloudy cores due to the presence of some iron oxides.
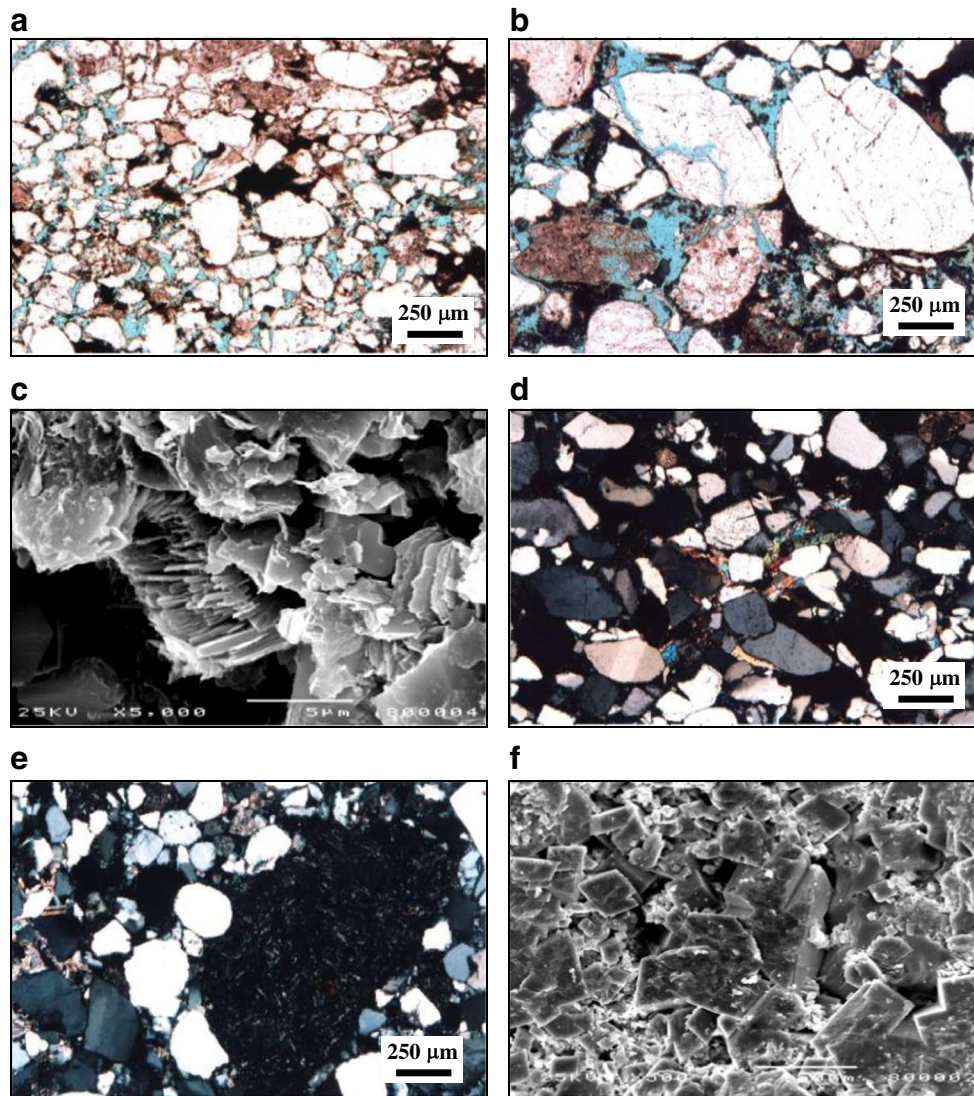
Fig. 3 Photomicrographs showing **a** very fine to medium-grained quartz with many altered feldspar grains, cemented together by ferruginated clay patches which slightly reduced the intergranular pore spaces, argillaceous subfeldspathic arenite microfacies, PPL and **b** fine to coarse quartz grains, sometimes are highly fractured, with many highly altered feldspars and good intergranular porosity. Note the presence of many ferruginous clay patches filling the pore spaces, argillaceous subfeldspathic arenite microfacies, PPL. SEM photomicrographs showing **c** kaolinite booklets partially filled the pore spaces, argillaceous subfeldspathic arenite microfacies, **d** fine to medium-grained quartz grains compacted together in suture and concave-convex contacts, with few altered feldspar grains. The grains are embedded in siliceous cement with some gypsum patches, siliceous quartz arenite microfacies, C.N., **e** Fine to medium-grained quartz grains, cemented together by silica with some gypsum patches. Sometimes, the pore spaces are completely filled with silica patches, siliceous quartz arenite microfacies, C.N., and **f** euhedral dolomite rhombs, well developed and interlocked together, filling the pore spaces, dolomitic sublithic arenite microfacies

Petrophysical studies

Conventional core analyses

Values of the petrophysical parameters obtained from the conventional core analyses of the studied Belayim sandstone samples and their interrelationships are the main key for discriminating the studied samples into petrophysical facies. For the present Belayim samples, they can be summed up into three petrophysical facies: Facies-1, Facies-2 and Facies-3. The petrophysical Facies-1 is composed mostly of argillaceous subfeldspathic arenite; Facies-2 is composed of siliceous quartz arenite, whereas the petrophysical Facies-3 is composed mostly of dolomitic sublithic arenite microfacies. Values of the different parameters obtained from the conventional core analyses are listed in Table 3.

Samples of Facies-1 are characterized by relatively high bulk density (of average 2.48 g/cm^3) and grain density values (of average 2.66 g/cm^3). Based on the classification ranks for the reservoir rocks that were proposed by Levorsen (1967) and modified by Nabawy et al. (2009a) and Nabawy (2015), porosity values (helium porosity '$\varnothing_{He}$' and summation fluid

porosity '$\varnothing_{SF}$') are ranked as negligible to fair of average poor values (av. $\varnothing_{He}$ = 6.47%, av. $\varnothing_{SF}$ = 7.38%), while the average horizontal and average permeability values are ranked as fair values (Table 3). The average permeability anisotropy (av. λ_k = 1.85) is ranked as moderate anisotropy (Nabawy and El-Hariri 2008; Nabawy et al. 2009b). Therefore, the average value of the RQI (av. RQI = 0.23) declares an impervious reservoir (0.0 < RQI ≤ 0.25), whereas the average value of the FZI (av. FZI = 3.40) declares a fair reservoir (2.5 < FZI ≤ 5.0; El Sharawy and Nabawy 2016).

The second petrophysical facies is characterized by good to very good porosity (av. $\varnothing_{He}$ = 21.3%, av. $\varnothing_{SF}$ = 18.5%) and very good permeability values (av. k_H = 231.7 and av. k_V = 215.4 md). The average permeability anisotropy (av. λ_k = 1.12) of Facies-2 is ranked as slight anisotropism. The RQI and FZI average values (0.81 and 2.81 μm, respectively) are ranked as fair values (0.5 < RQI ≤ 1.0, 2.5 < RQI ≤ 5.0; El Sharawy and Nabawy 2016).

Samples of Facies-3 are characterized by relatively high grain density 'σ_g' values (av. σ_g = 2.71 g/cm^3 which is diagnostic for the carbonate rocks). Porosity of the present samples is ranked as fair values (av. $\varnothing_{He}$ = 12.7%, av. $\varnothing_{SF}$ = 11.1%) with good permeability values (av. k_H = 43.3 and av. k_V = 30.6 md) and slight permeability anisotropy (λ_k = 1.15).

Though their good storage capacity properties (average RQI and FZI values are equal to 0.43 and 2.80 μm, as respectively), the studied rock samples are ranked as poor (0.25 < RQI ≤ 0.5) to fair (2.5 < FZI ≤ 5.0) reservoir rocks.

The petrophysical properties of the Belayim samples are studied further through applying a number of *X-Y* plots to reveal the interrelationships between these parameters and to introduce a number of empirical equations that can be applied for calculating a missed parameter in terms of the other.

Grain density σ_g as a function of bulk density σ_b

The grain density σ_g is a direct indication for the mineral composition of the studied rocks, whereas the bulk density σ_b is an indication of both the pore volume and the mineral composition, i.e. it is the net result of both the grain density and porosity. Therefore, plotting the σ_g as a function of the σ_b is a main key for discriminating the present sandstone samples into three facies based on their mineral composition, porosity and density (Fig. 4). The measured densities for samples of Facies-1 and Facies-2 are characteristic for arenite composition ($\sigma_g \approx$ 2.65 ± 0.03 g/cm^3) except for samples of Facies-3 (dolomitic sublithic arenite microfacies) which shift up towards the dolomitic composition (σ_g values approaches up to 2.84 g/cm^3). However, as revealed from the petrographical studies, the presence of some iron oxide patches may slightly increase the grain density values. It also reveals that there is a good discrimination between the bulk density values of both
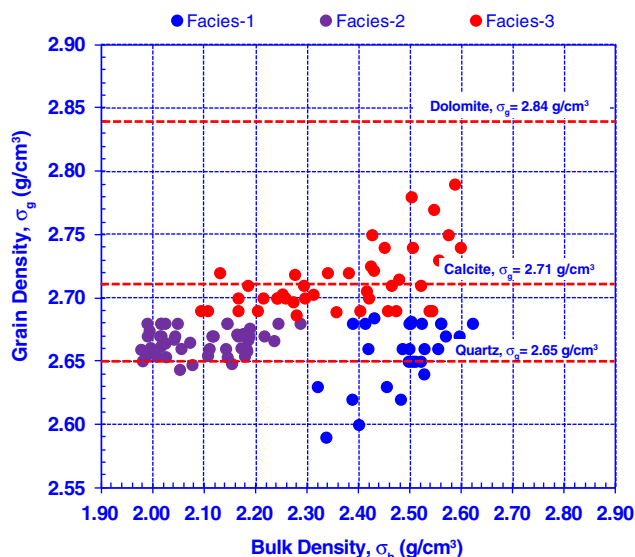

Fig. 4 Plotting the bulk density 'σ_b' as a function of the grain density 'σ_g' for the studied Belayim petrophysical facies, Gulf of Suez, Egypt

the Facies-1 and Facies-2, whereas Facies-3 (the dolomitic samples) has a wide range of bulk density values.

Porosity $\varnothing_{He}$ and $\varnothing_{SF}$ as a function of the bulk density σ_b

For the present study, plotting porosity $\varnothing_{He}$ as a function of the bulk density is used as a quality control plot, where it is of excellent reliability ($r \leq -0.950$, for the different relationships) between both parameters (Fig. 5a). It is worth to mention that both the constant value and multiplication factor of the $\varnothing_{He}$-σ_b empirical equations (Fig. 5a) increase gradually from Facies-1 (argillaceous samples) to Facies-2 (the siliceous samples). The relationship between $\varnothing_{SF}$ and σ_b is more disturbed than that with the $\varnothing_{He}$ (Fig. 5b).

Permeability k_H and k_V as a function of porosity $\varnothing_{He}$ and $\varnothing_{SF}$

Permeability *k* or what we can call 'the hydraulic conductivity' is a direct contribution for the effective porosity and its pore types, so plotting permeability as a function of porosity may be a direct indication for the hydraulic connectivity of the pore spaces and their pore throat distribution. For the studied samples, porosity was measured by two methods, the summation fluid and helium porosity ($\varnothing_{SF}$ and $\varnothing_{He}$) techniques, and also, the permeability was measured in two directions: vertical and horizontal (k_V and k_H). Both types of permeabilities were plotted as a function of both types of porosities (Figs. 6 and 7).

Plotting k_H as a function of $\varnothing_{He}$ is more reliable than its plotting as a function of $\varnothing_{SF}$. Also, plotting permeability in the vertical direction k_V as a function of porosity ($\varnothing_{He}$ and $\varnothing_{SF}$) is relatively less reliable ($0.646 \leq r \leq 909$, for the different relationships) than plotting the permeability in the horizontal direction k_H with the porosity data obtained from both methods
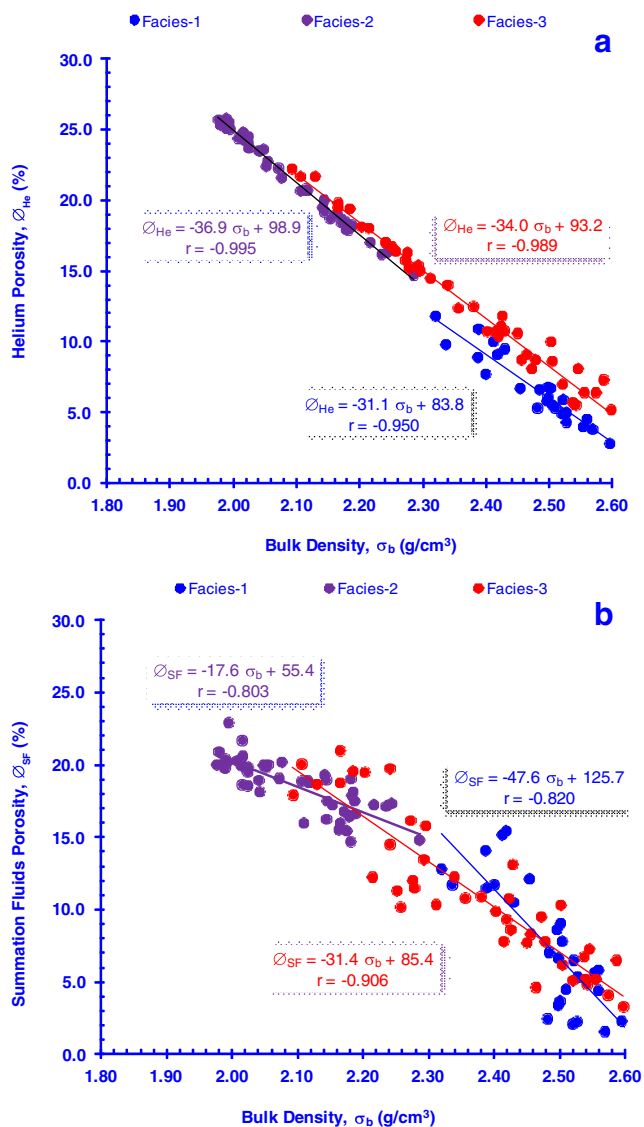
Fig. 5 Plotting the bulk density 'σ_b' as a function of **a** porosity measured using the helium injection '$\varnothing_{He}$' and **b** porosity measured using the summation fluid technique '$\varnothing_{SF}$' for the studied sandstone samples
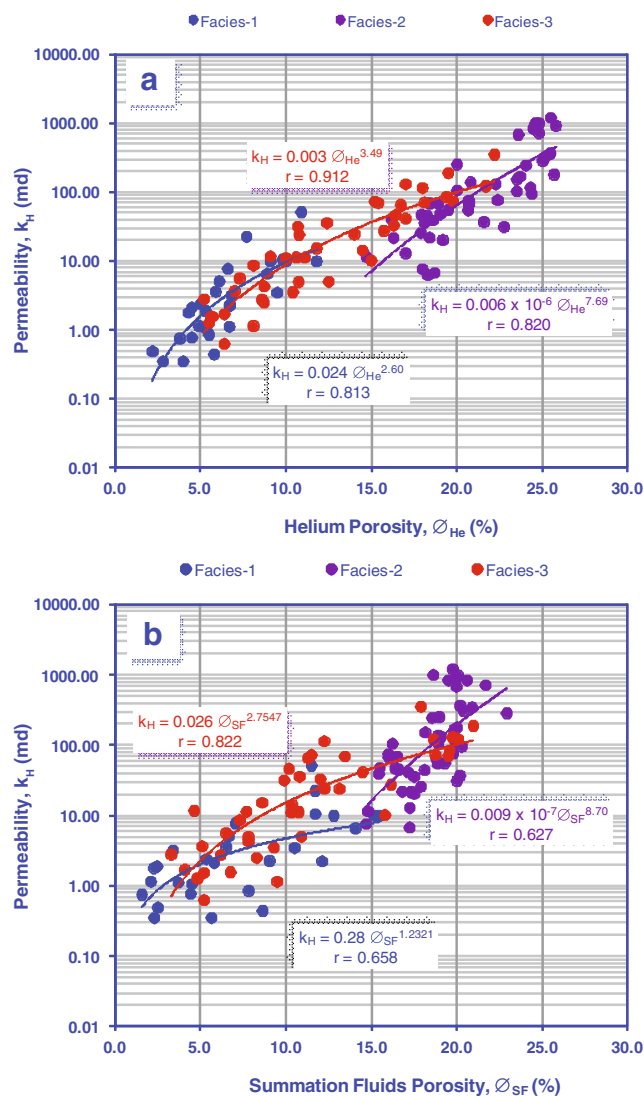

Fig. 6 Plotting the gas permeability 'k_H' of the studied samples measured in the horizontal direction as a function of porosity measured by **a** helium porosity technique '$\varnothing_{He}$' and **b** summation fluid porosity '$\varnothing_{SF}$' technique

($0.627 \leq r \leq 912$, for the different relationships). Sometimes, plotting the k_V values as a function of $\varnothing$ is more reliable than plotting the k_H values as a function of $\varnothing$ due to the presence of some vertical fracture systems.

Reservoir quality index as a function of σ_b, $\varnothing_{He}$ and k_H

The RQI for the present study was calculated using the horizontal permeability k_H and the helium porosity $\varnothing_{He}$. Plotting the RQI as a function of σ_b and $\varnothing_{He}$ indicates that it can be calculated in terms of both parameters in reliable exponential relationships (Fig. 8a, b) with their power less than −8.4 down to −12.1 for the bulk density (Fig. 8a) and between 0.80 and 3.34 for the helium porosity (Fig. 8b). Plotting the RQI as a function of permeability k_H indicates that the permeability is a

main contributor for the RQI with an excellent reliability ($r \geq 0.972$, for the different relationships) as well as similar exponent values and multiplication factors for both Facies-1 and Facies-3 (Fig. 9).

Flow zone indicator as a function of σ_b, $\varnothing_{He}$ and k_H

The FZI is a parameter that can be used in addition to the RQI to discriminate and slice the reservoir rocks into flow units. Plotting the FZI values of Facies-1 and Facies-3 samples as a function of the bulk density, porosity and permeability has a weak to very weak reliability ($r \leq 0.55$, for the different relationships) which indicates that the FZI data are mostly highly scattered than the RQI data. However, samples of Facies-2 show an excellent reliability for plotting FZI as a function of permeability ($r = 0.977$, for the different relationships, Fig. 9).
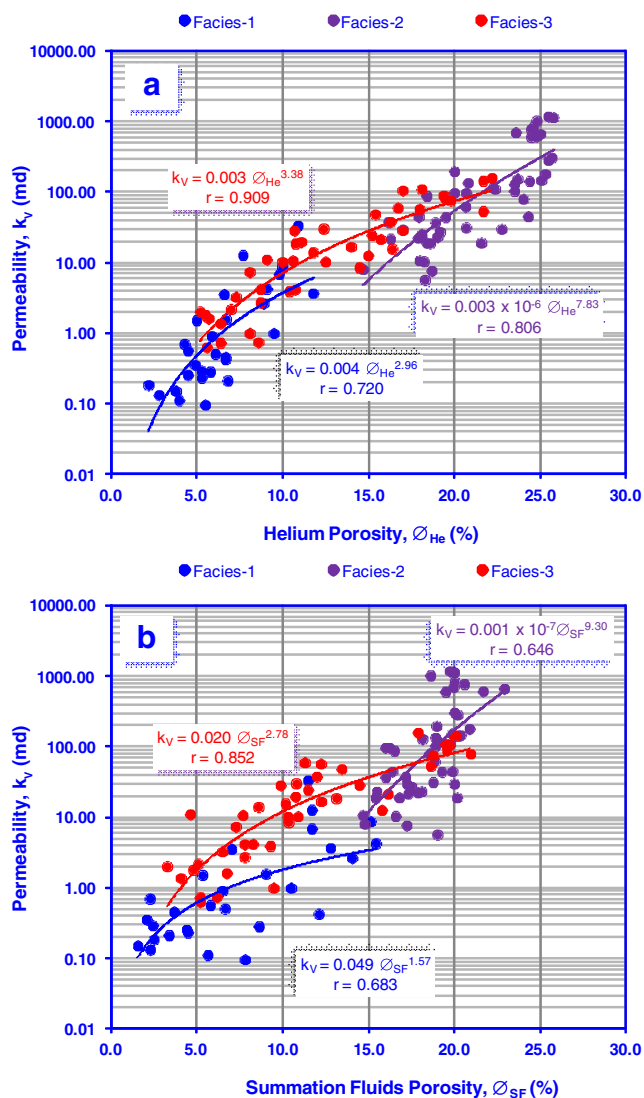
Fig. 7 Plotting the gas permeability 'k_V' of the studied samples measured in the vertical direction as a function of porosity measured by **a** helium porosity technique '$\varnothing_{He}$' and **b** summation fluid porosity '$\varnothing_{SF}$' technique

Reservoir zonation and discrimination

To evaluate the petrophysical potential of the studied Belayim reservoir zones, the RQI and FZI of Amaefule et al. (1993) as well as the RPI accompanied with the porosity values ($\varnothing_{SF}$, $\varnothing_{He}$), the permeability values (k_H, k_V) as well as the water (Sw) and the oil (So) saturation were plotted as a function of depth (Fig. 10). This plot is the main key for slicing and discriminating the studied sequence into conductive and super conductive reservoir zones.

The conductive reservoir zones were determined using porosity and permeability cut-offs equal to 10% and 10 md, respectively. The permeability anisotropy cut-off was taken to be less than 2.0 as an indication for the homogeneity of the reservoir flow properties. This vertical plot enabled zonation of the studied reservoir into different flow units. The upper

flow unit 'FU1' represents the cored interval of zone IIA (14.0 m) of Hammam Faraun member, whereas zone IV of Sidri member can be sliced into five flow units (FU2 to FU6); two of them are characterized by fair to very good reservoir properties (FU3 and FU5) of total thickness 9.0 m (Fig. 10). The other three flow units (FU2, FU4 and FU6) are impervious or characterized by poor reservoir properties ($\varnothing < 10\%$, $k < 10$ md, RQI < 0.5 and/or FZI < 2.5) and not considered as potential reservoir units. These flow units are mostly saturated with water up to 90%.

To characterize the super conductive reservoir zones, it is recommended to use the same cut-off values but with $k \geq 100$ md, RQI ≥ 1 μm, FZI ≥ 5 μm and RPI ≥ 3. Using these cut-offs indicates that only thin zone 'FU3' (3.0 m, Fig. 10) of Sidri member can be assigned as super conductive zone characterized by very good permeability and good to very good RQI, FZI and RPI.

In addition, plotting the RQI as a function of FZI (Fig. 11a) can be used as a tool for ranking the quality of the reservoir samples (El Sharawy and Nabawy 2016). This plot indicates that most values of the studied samples of Facies-1 are characterized by poor to impervious RQI values (0.09 ≤ RQI ≤ 0.68, av. RQI = 0.23) and poor to fair FZI values (1.04 ≤ FZI ≤ 6.59, av. FZI = 3.40), i.e. it is mostly considered as non-reservoir facies. On the other side, the samples of Facies-2 are mostly characterized by fair to very good RQI values (0.18 ≤ RQI ≤ 2.15, av. RQI = 0.81) and fair to good FZI values (0.82 ≤ FZI ≤ 6.28, av. FZI = 2.81). The samples of Facies-3 are considered as a transitional group, in their petrophysical potential, between samples of Facies-1 and Facies-2. In addition, this plot can be used as a tool for discriminating the studied sequence into reservoir and non-reservoir flow units (Fig. 11b). Some non-reservoir streaks are noticed in FU5 represented by samples characteristic with RQI values less than 0.5 μm and/or FZI values less than 2.5 μm.

Special core analyses

The special core analyses are additional procedure for discriminating the reservoir into petrophysical facies and flow units. It has a great importance for measuring the Archie's parameters a, m and n (Archie 1942) as well as to check the effect of the confining pressure on the petrophysical parameters. In addition, studying the pore throat distribution of the studied samples is the key control for the fluid flow through the different flow units.

Formation resistivity factor and porosity $\varnothing_{He}$ relationship

The lithology factor a and the porosity $\varnothing$ exponent m of Archie's eq. (FR = a × $\varnothing^m$) are mostly controlled by the architecture of the studied rocks represented by the pore
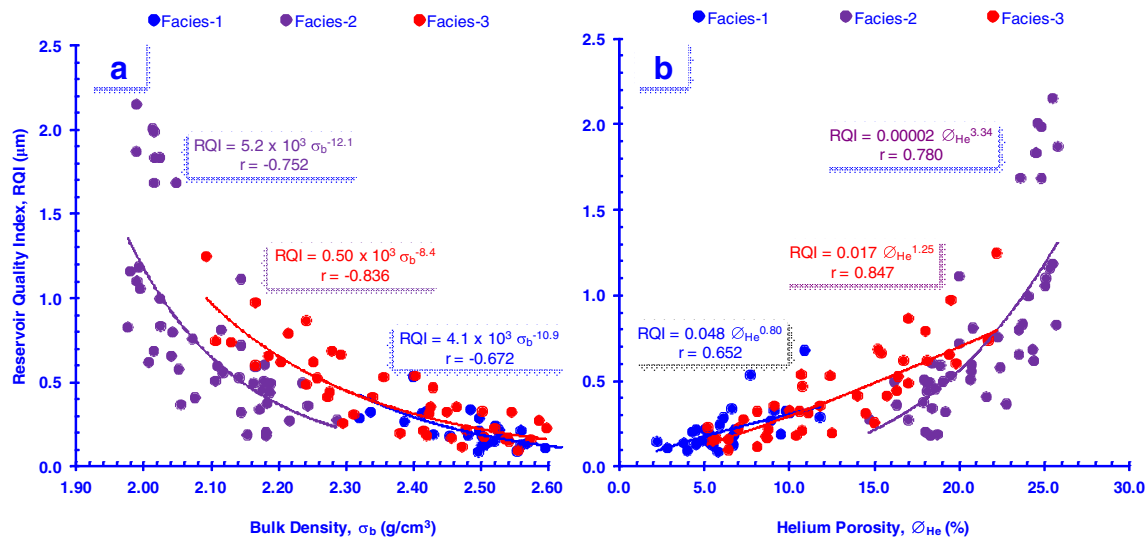
Fig. 8 Plotting the reservoir quality index (RQI) as a function of **a** the bulk density 'σ_b' and **b** the helium porosity '$\varnothing_{He}$' of the studied samples

fabrics and petrofabrics. Porosity exponent m is mostly dependent on the pore fabric including the pore volume as well as the pore elongation and foliation in 3D, whereas lithology factor a is dependent mostly on the lithology, grain-to-grain relationship, permeability and porosity; i.e. on both pore fabrics and petrofabrics (Nabawy 2015). The two aforementioned parameters a and m, in turn, control the FR-$\varnothing$ relationship.

To calculate the Archie's parameters a and m, the FR factor was plotted as a function of porosity $\varnothing_{He}$. The present technique was applied for samples of Facies-2 and Facies-3 (as hydrocarbon prospective facies. Based on the classification introduced by Nabawy (2015), the calculated 'FR' is very low for the siliceous samples of Facies-2 (FR ≤ 50) and low for samples of Facies-3 (50 ≤ FR ≤ 150, for the different

facies) with excellent and good average porosity for the studied facies, respectively (Table 4).

The reliability of the obtained relationships is very high for both facies (−0.994 ≤ r ≤ −0.996, for the different relationships, Fig. 12). The lithology factor a values are discriminative between both facies, where it is 1.09 for the clastic samples of Facies-2 and 2.47 for the dolomitic samples of Facies-3. This is in consistence with that stated by Nabawy (2015) who mentioned that the dolomitic samples are characterized by relatively high a values. He added that a is mostly inversely related to m where the pore fabrics and petrofabrics are two supplementary fabrics for the whole rock. Therefore, the porosity exponent m is relatively higher for the samples of Facies-2 ($m = 1.58$) than that for the dolomitic samples of Facies-3 ($m = 1.14$). On the other side, considering a as a constant value equal to the unity, so m can be studied as a variable value and has to be calculated for each sample. The average m value for Facies-2 samples (av. $m = 1.64$) is higher than that for Facies-3 samples (av. $m = 1.56$, Table 4).

Effect of pressure on FR and porosity values

The effect of the confining pressure on the formation resistivity factor and Archie's parameters is studied at average pressure 6100 psi for zone IIA and 6300 psi at zone IV. Increasing the applied pressure causes more closure for the pore throats. So, it was expected to get higher a values and lower m values. The effect of pressure on m values is more detectable with the variable m which increased with increasing the applied pressure (Fig. 12).

The effect of the confining pressure on the FR factor is attributed mostly to its effect on porosity value $\varnothing$, i.e. to its
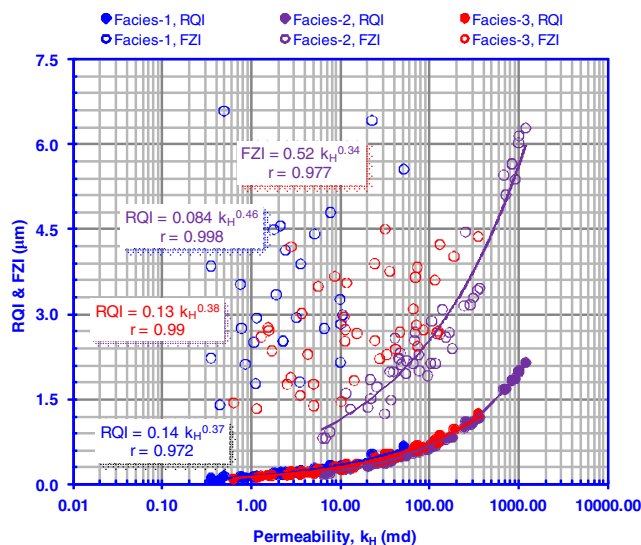

Fig. 9 Plotting the permeability of the studied samples measured in the horizontal direction 'k_H' as a function of **a** reservoir quality index (RQI) and **b** flow zone indicator (FZI)
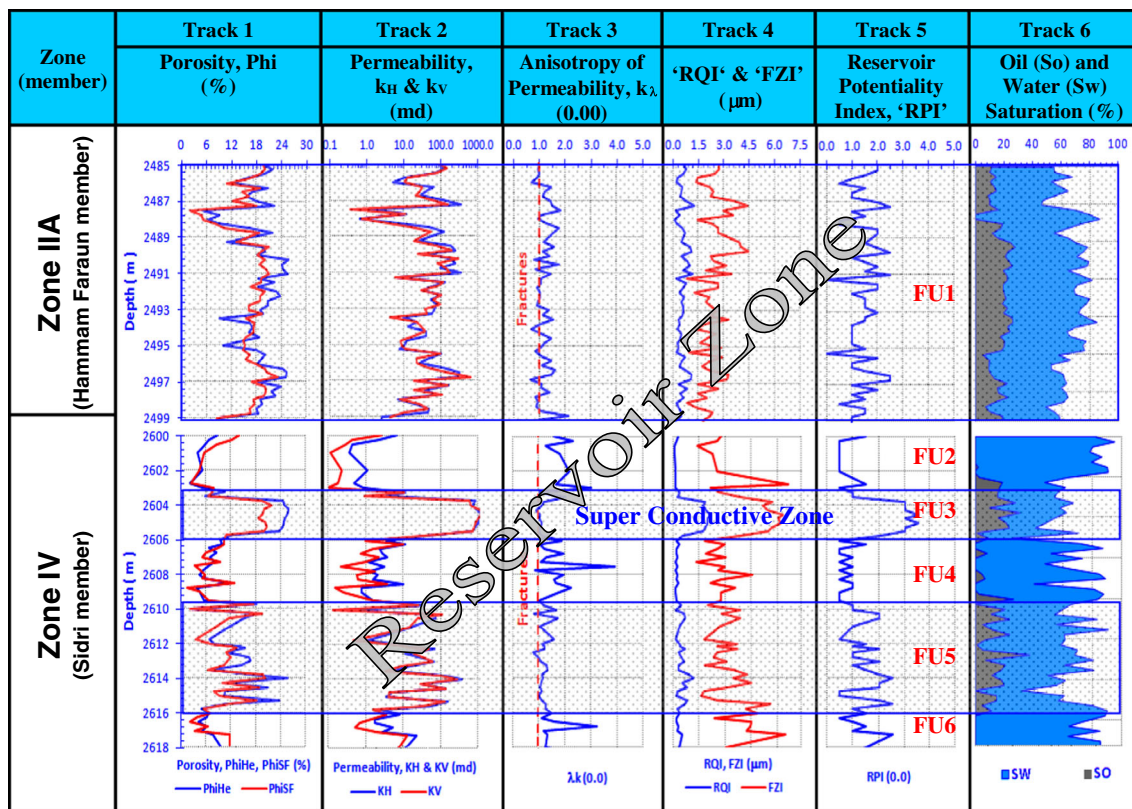
Fig. 10 Vertical matching of the routine core analyses data and the reservoir quality parameters of the Belayim Formation in the Belayim onshore oil field, Gulf of Suez, Egypt. The studied reservoir zone can be defined into 6 flow units 'FU1–6'

effect on the pore throat distribution and the electric conductivity. Porosity was measured again at fixed points of incremental increase of the confining pressure 'P' up to 6000 psi, and the PR was calculated at the final confining pressure (Fig. 13, Table 5). The relationship between both parameters can be expressed by an inverse exponential relationship as follows.

$$\varnothing = a \Big/ P^b \qquad (8)$$

where a is a multiplication factor that varies between 22.1 and 33.1 for the samples of Facies-2 and between 7.1 and 21.5 for the samples of Facies-3, whereas b is an exponent for P that varies from 0.023 to 0.061 and 0.015 to 0.037 for both facies, respectively.

It is indicated that both the multiplication factor and the exponent values are higher for the studied samples of the siliceous Facies-2 than that for the dolomitic Facies-3. Moreover, the PR for the samples of Facies-2 (Fig. 13a) is mostly higher than that for Facies-3 samples (Fig. 13b).

Plotting resistivity index as a function of Sw_{irr}

The apparent resistivity was measured at 100% saline water saturation; then, the irreducible water saturation

'Sw_{irr}' was measured for each sample of the studied Facies-2 and Facies-3, and the true electric resistivity was measured at the Sw_{irr}, and the RI can be calculated. The Sw_{irr} for the studied samples is mostly similar for both facies (26.1–34.7%), whereas the average RI for Facies-2 is relatively higher (RI = 18.7) than that for Facies-3 (RI = 10.6) (Table 4).

The variable saturation exponent n was calculated for each sample (Fig. 14a, b); it varies between 2.10 and 2.29 for the samples of Facies-2 which is relatively higher than that for the samples of Facies-3 ($1.82 \le n \le 1.99$, for the studied samples). On the other side, processing n as a constant value for each facies means a plot of the RI at Sw_{irr} for each sample on X-Y plot; then, the slope and intercept were calculated (Fig. 15). The saturation exponent n for Facies-2 ($n = 2.29$) is higher than that for Facies-3 ($n = 1.92$). To detect the relationship between both the saturation exponent n and the porosity exponent m for each sample, n value for each sample was presented as a function of its correspondence m value (Fig. 16). It is clear that there is an inverse proportional relationship between both parameters, where the n value can be calculated in terms of m, with a reliability ($r \le -0.730$, for the different relationships) using the following empirical relationships.

$$\text{Facies} - 2, n = 2.08 \Big/ m^{0.086} \quad (r = -0.824) \qquad (9)$$

Fig. 11 Plotting the reservoir quality index (RQI) of the studied samples as a function of the flow zone indicator (FZI) taken into consideration **a** the petrophysical facies and **b** the flow units
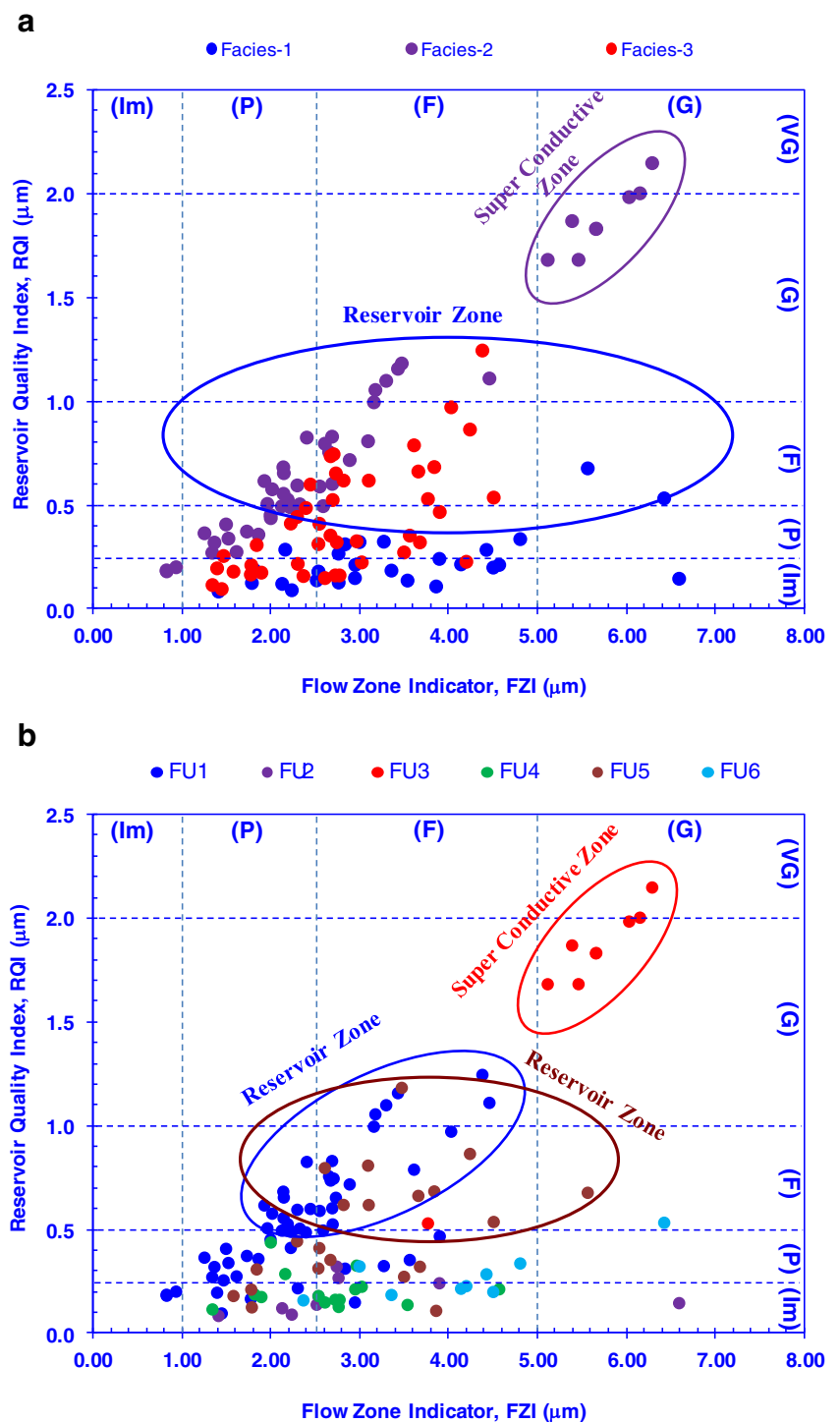
$$\text{Facies}-3, n = 5.26 / m^{1.619} \quad (r = -0.730) \tag{10}$$

The multiplication factor and the exponent are higher for the dolomitic samples of Facies-3 than that for the siliceous samples of Facies-2.

Plotting the gas and liquid permeabilities 'k$_G$ and k$_L$' as a function of ∅

In a trial to define the micropore spaces that are not accessible to water injection, the permeability was measured by two methods, by the gas k_G and water flow k_L. The values of k_G
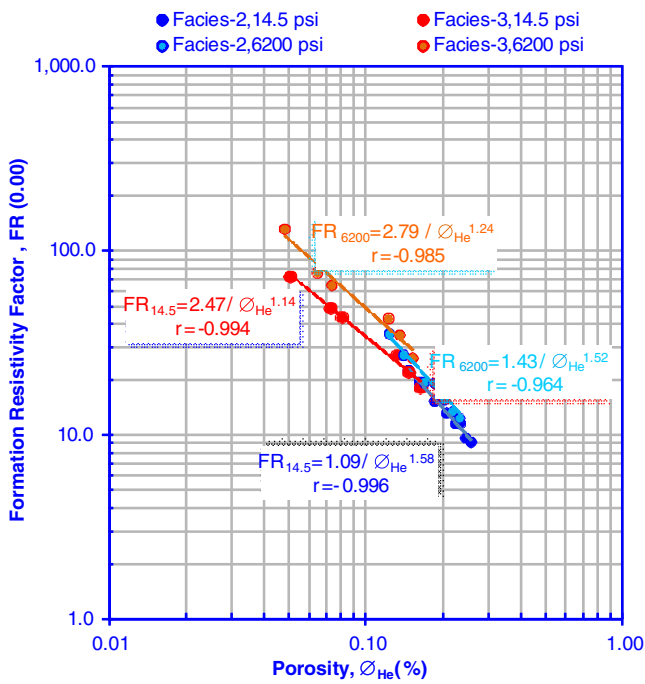
Fig. 12 Plotting the formation resistivity factor (FR) as a function of porosity measured by helium injection '$\varnothing_{He}$' at ambient pressure (14.5 psi) and at high pressure (6200 psi)

Fig. 13 Effect of the overburden pressure on the studied samples causing porosity reduction (PR) for **a** the siliceous quartz arenite samples and **b** the dolomitic sublithic arenite samples

are always higher than that for the k_L (Table 5, Fig. 17). The difference between both values reveals the value that is attributed by micropores and nanopores that are not accessible to the water flow, i.e. do not contribute to the liquid permeability (Table 5). It can be expressed by 'k_μ' which can be calculated as follows.

$$k_\mu = 100 \times (k_G - k_L) \big/ k_G \qquad (11)$$

This difference is lower for the samples of Facies-2 ($k_\mu = 43.1\%$) than that for the samples of Facies-3 ($k_\mu = 54.1\%$). The porosity exponents for the 'k-$\varnothing$' relationships are lower for the samples of Facies-2 (2.48 and 2.74 for the k_G-$\varnothing$ and k_L-$\varnothing$, respectively) than that for samples of Facies-3 (4.07 and 4.59 for the k_G-$\varnothing$ and k_L-$\varnothing$, respectively).

Relationship between the 'k_{rw} and k_{ro}' and the Sw_{irr} as a tool for measuring the wettability

The wettability was measured for the studied samples using the Amott technique as the difference between the wettability of rock to water and its wettability to oil. When the wettability of the rock sample to water is greater than that to the oil, therefore the rock is considered as water wet and will have positive Amott index (AI); otherwise, it is considered as oil wet and will have negative Amott index. The grade of the wettability
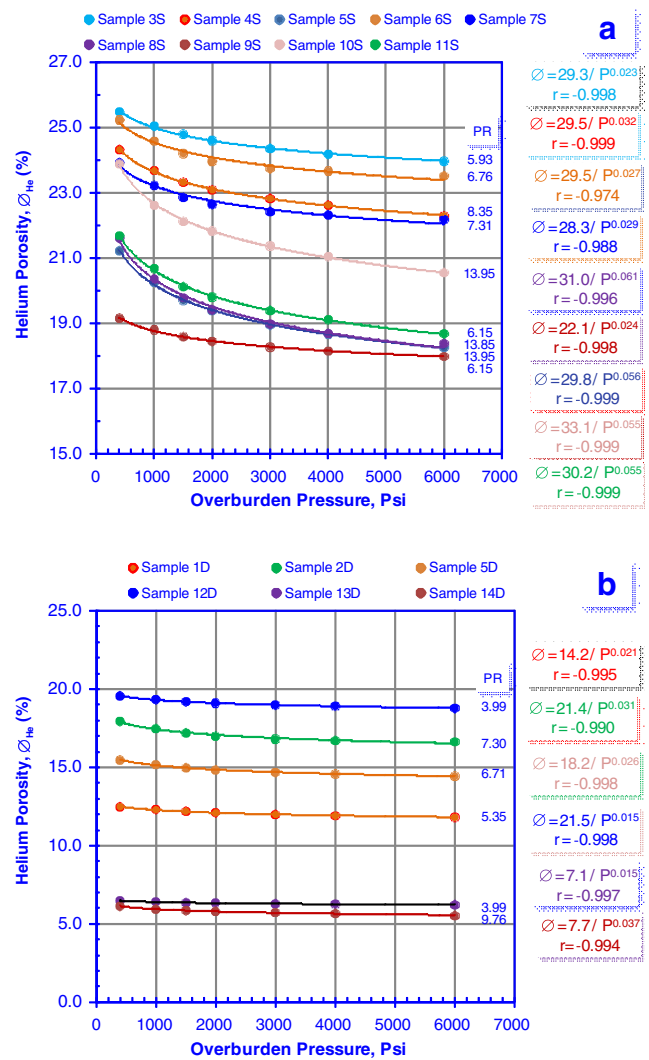
value is ranked as shown in Table 1. Most of the studied samples of Facies-2 are considered as moderately oil wet to neutral wet (Table 6), whereas most of the studied samples of Facies-3 are strongly to weak oil wet. Few samples are characterized by weak water wettability due to its high Sw_{irr} and low So_r values. On the other side, the strongly oil wet samples are characterized by the highest So_r and the lowest Sw_{irr} values (Table 6).

In addition, plotting the relative permeability values (k_{ro} and k_{rw}) of the studied samples as a function of increasing the water saturation Sw as a wetting phase and the oil saturation So as a non-wetting phase is an additional tool for defining the wettability of the studied rocks. The moderately oil wet samples are characterized by relatively high k_{rw} ($k_{rw} \geq 0.6$) and relatively low Sw_{irr} ($0.2 \geq Sw_{irr}$), whereas the weak water wet samples are characterized by relatively low k_{rw} ($k_{rw} \leq 0.4$) and relatively high Sw_{irr} ($0.3 \leq Sw_{irr}$). Most of the studied samples
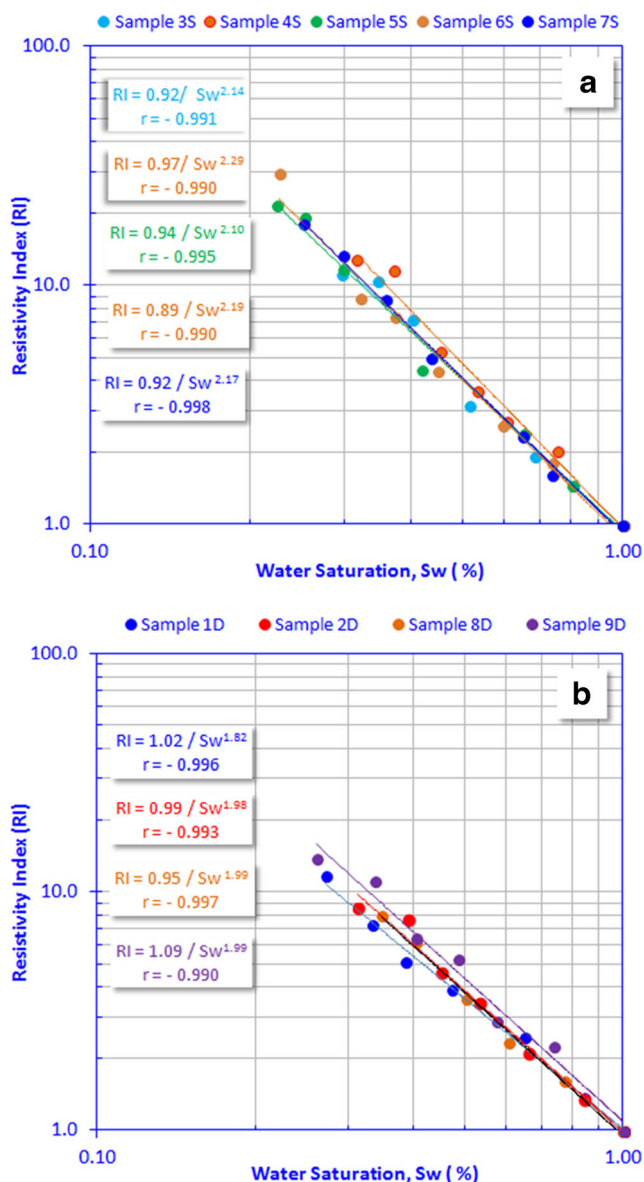
Fig. 14 Determination of the saturation exponent 'n' for each sample by plotting the resistivity index (RI) as a function of the water saturation 'Sw' (where 'n' is the exponent of 'Sw') for each sample **a** the siliceous quartz arenite samples and **b** the dolomitic sublithic arenite samples
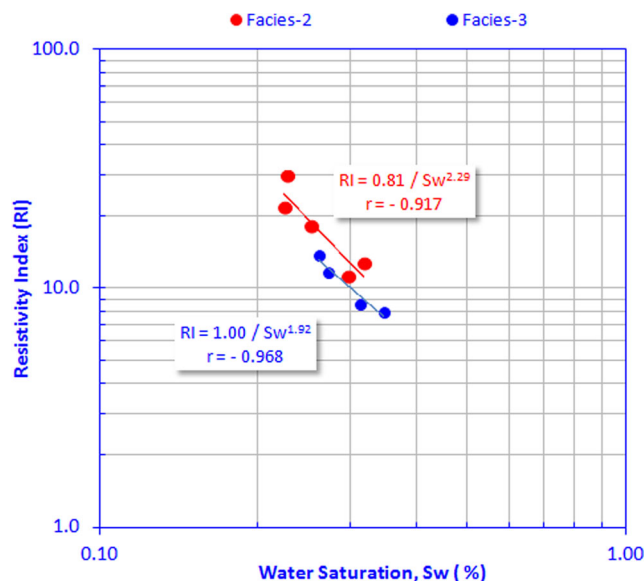

Fig. 15 The determination of the saturation exponent 'n' for the studied facies

by an abrupt increase in porosity values' threshold stage ($10 \geq D \geq 1.0$ μm, mesopores) and finished by another more or less steady stage (1.0 μm $\geq D$, micropores and nanopores).

Nabawy et al. (2009a) classified the highly porous Nubia sandstones in south Egypt into four ranks based on the behaviour of the pore throat distribution curve and based on the extension of these three stages. For the present study, the obtained curves are not compatible with the classification proposed by Nabawy et al. (2009a). Therefore, for the present study, it is proposed to discriminate the quality of the studied samples based on the percentage of the measured pore diameters as shown in Table 2, where a new classification is proposed based on the published data for the highly porous Nubia
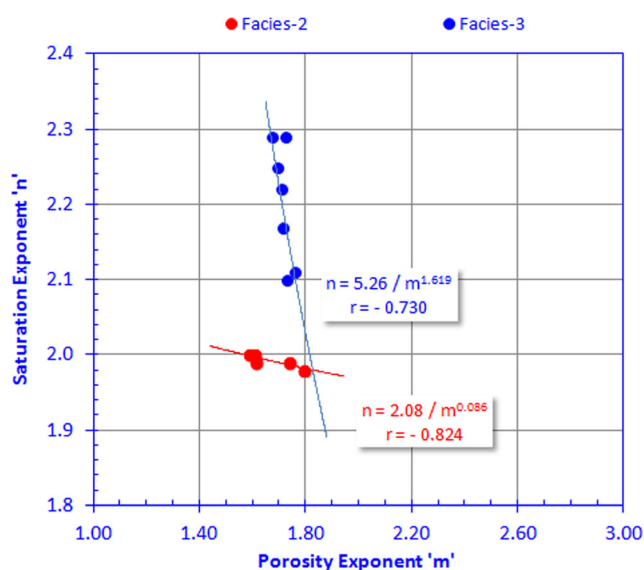
are described as moderately oil wet to neutral with few water wet samples as an exception (Fig. 18).

The pore throat distribution

To determine the quality of the studied reservoir samples, the pore throat radii were plotted as a function of the accumulative porosity measured by mercury injection (Fig. 19). The studied pore throat distribution for the different samples is characterized by a steady stage with negligible porosity fraction (pore diameter 'D' ≥ 10 μm, megapores and macropores) followed

Fig. 16 Presenting the saturation exponent 'n' as a function of the porosity exponent 'm' for samples of Facies-2 and Facies-3
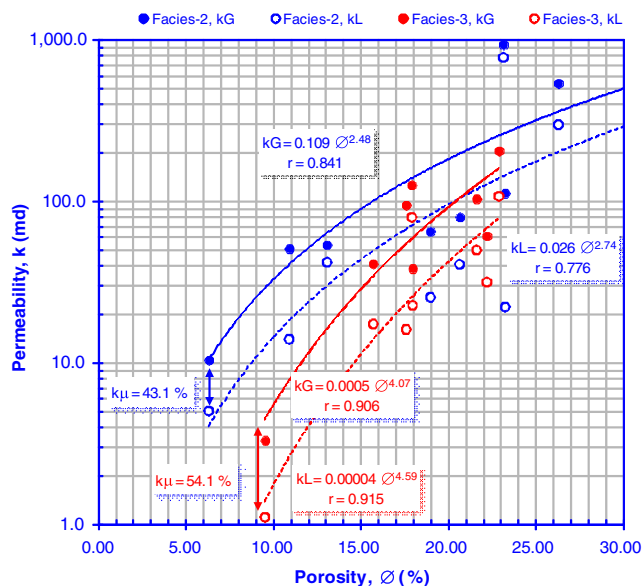
Fig. 17 Plotting the liquid and gas permeabilities (k_L and k_G) of the studied samples as functions of porosity. Note that the average contribution of the micropores in the bulk gas permeability is indicated by 'k_μ'

sandstone samples as well as the present data. The classification consists of six reservoir ranks (rank I to rank VI).

The proposed classification was useful for characterizing the studied samples into four ranks as shown in Fig. 19. The studied samples of Facies-2 and Facies-3 are characterized by good to very good porosity, good permeability, relatively low threshold pressure ($\leq$12.2 psi) and $\approx$75% mesopores and macropores (Table 7). Therefore, the samples of Facies-2 are described as rank III (macropores $\geq$75% and micropores <25.0%), whereas the samples of Facies-3 belong to rank IV (macropores <75% and micropores $\geq$25.0%, Fig. 19a, b, respectively).

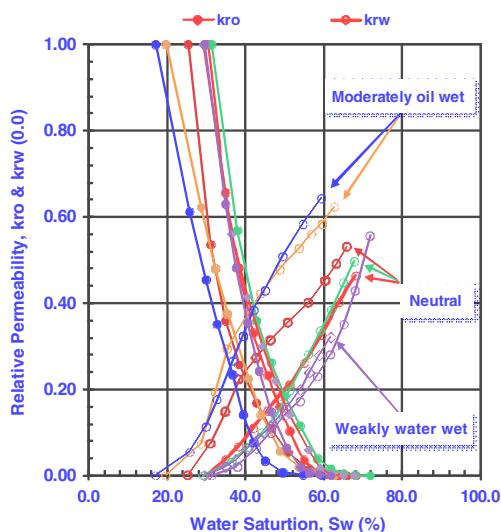**Fig. 18** Presenting the relative permeability of oil 'k_{ro}' and water 'k_{rw}' as a function of the water saturation 'Sw' as an indication for the wettability

On the other side, the samples of the argillaceous Facies-1 are characterized by poor porosity, fair permeability, relatively high threshold pressure ($\geq$77.5 psi) and absence of megapores and macropores. So, these samples are ranked as rank V (mesopores $\geq$50% and micropores <50.0%) and rank VI (mesopores <50% and micropores $\geq$50.0%) (Fig. 19c, d, respectively).

General discussion

The petrophysical properties of a given reservoir rocks can be defined as its physical properties based on its pore volume and connectivity as well as its pore fabrics and petrofabrics. The pore volume and the rock fabric of the given rock (including the pore fabric and petrofabrics) are mostly controlled by the diagenetic history of that rock. Therefore, the petrophysical properties and the quality of a studied reservoir are mostly controlled by its mineral composition and diagenetic history including the porosity-enhancing and porosity-reducing diagenetic factors.

For the present Belayim sandstones, the studied samples are divided petrographically into three microfacies based on their mineral composition: (1) argillaceous subfeldspathic arenite, (2) siliceous quartz arenite and (3) dolomitic sublithic arenite microfacies. Though all samples are arenites, their cement material seems to play an important role in their petrophysical behaviour giving rise to three different petrophysical behaviours based on the argillaceous, siliceous and dolomitic cement.

Petrophysically, Facies-1 is characterized by the least petrophysical potential with ranks V and VI as mentioned from the pore throat distribution with neither megapores nor macropores and more than 25% micropores and nanopores and the rest are mesopores. Petrographically, it is composed mostly of argillaceous subfeldspathic with many argillaceous patches and altered feldspars giving rise to many authigenic kaolinite accumulations stacked in the pore throats (Fig. 3c). The argillaceous content reduced the petrophysical potential by reducing the pore volume to less than 10% represented mostly by matrix porosity and microfractures. The RQI values are relatively low and described as impervious to poor rocks (0.09 $\leq$ RQI $\leq$ 0.68, Table 3, Fig. 11a, b). This argillaceous microfacies belongs mostly to the top and middle parts of FU2 and FU4 of Sidri member which are not considered as reservoir due to their poor petrophysical properties. Plotting the FZI values as a function of permeability k indicates a high data scattering and disturbance of this relation (Fig. 9). This may be attributed to heterogeneity in the distribution of the authigenic argillaceous material, i.e. a disturbance in their impact on the petrophysical potential and behaviour. This high disturbance can be checked by high permeability anisotropy

Fig. 19 Examples of the different reservoir ranks assigned using the data of the pore throat distribution obtained from the MICP technique applied for the studied Belayim sandstones
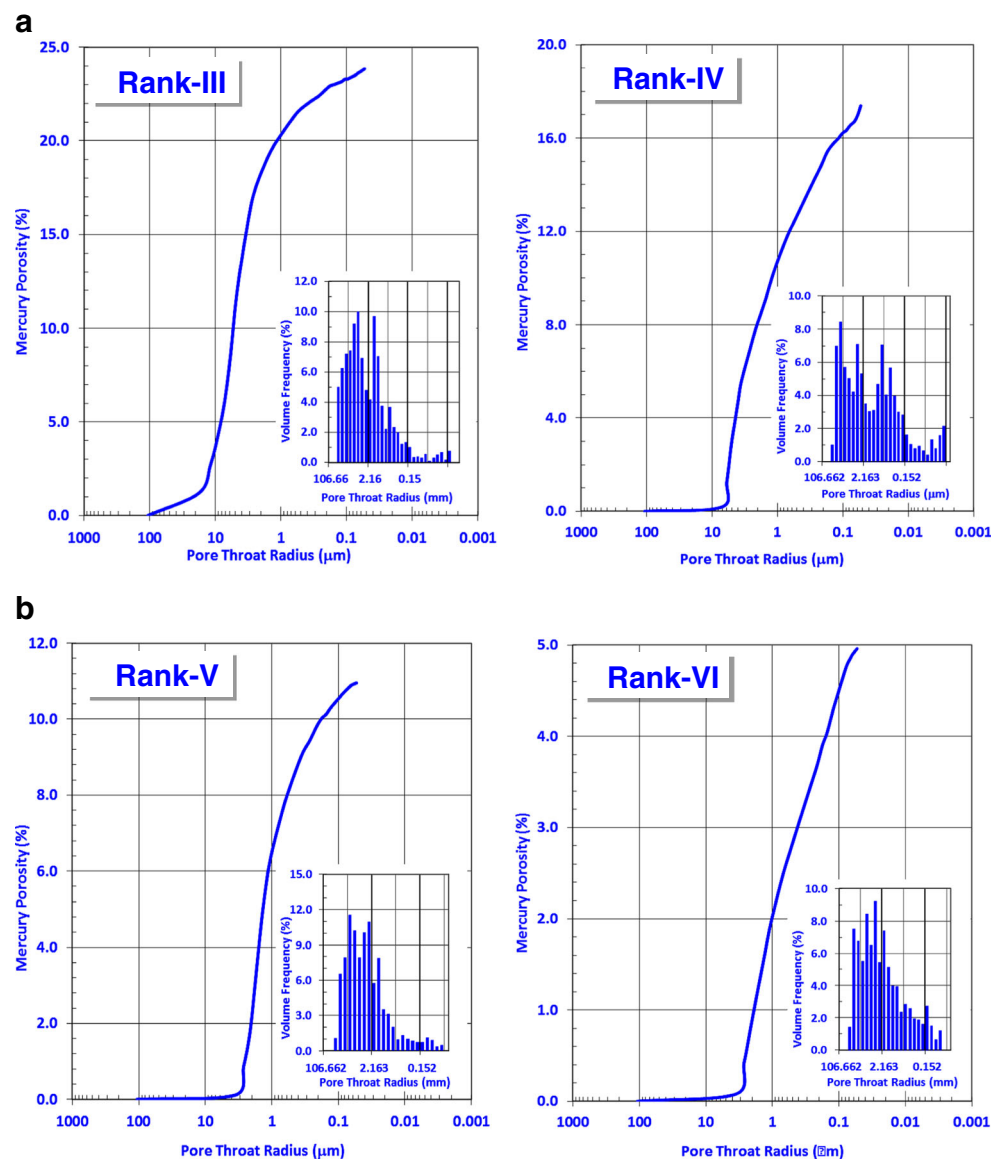
λ_k that reaches up to 3.89 with average of 1.85 which is relatively higher than λ_k for the other facies.

On the other side, the samples of the petrophysical Facies-2 are composed mostly of siliceous quartz arenite that are representative to the first flow unit FU1 of Hammam Faraun member and FU3 of Sidri member (FU3, Fig. 10). The petrophysical properties of this microfacies are the best rank between the studied microfacies of Belayim Formation. It is mostly characterized by slight siliceous cementation due to prevailing of porosity-enhancing diagenetic factors (e.g. dissolution and leaching out as well as fracturing). Though the quartz grains of these samples suffered from compaction for a long time (Fig. 3d, e), its impact on the petrophysical potential of this microfacies is not so much and they are still prospective for hydrocarbons. It is characterized by very good average porosity (av. $\varnothing_{He} = 21.3\%$, av. $\varnothing_{SF} = 21.3\%$) and very good

average permeability (av. $k_H = 231.7$, av. $k_V = 215.4$, Figs. 5, 6 and 7, Table 3). The high petrophysical potential of the siliceous facies is reasonably accompanied with fair to very good RQI (av. RQI = 0.81 μm) and fair to good FZI (av. RQI = 2.81 μm, Table 3, Fig. 11a). The very good storage capacity properties of this facies are accompanied with very low FR factor ($9.2 \leq FR \leq 22.6$, Table 4, Fig. 12). The porosity exponent values of m which are assigned in the ambient and confining pressures fluctuate around 1.55 which is diagnostic for this facies from that of Facies-3 (the dolomitic microfacies).

Checking the effect of confining pressure on porosity indicates that the siliceous facies is more sensitive for increasing pressure than that of the other facies where the PR may reach to 13.95% of the porosity value at the ambient conditions (Table 5, Fig. 13a). This may be attributed to the brittle nature

of the siliceous cement which causes its fracturing and collapse of pore spaces with increasing pressure, whereas the argillaceous and dolomitic cements can prohibit that effect. The multiplication factor and the pressure exponent of the '∅-P' relationship are diagnostic for this siliceous facies from that of the dolomitic one with much higher values (Table 5, Fig. 13a).

It is characterized by a relatively high saturation exponent n of average 2.18 which is also diagnostic for this petrophysical facies from the dolomitic Facies-3. This high n value is accompanied with relatively high RI values which can be attributed to relatively high true electric resistivity Rt, i.e. relatively low Sw_{irr} values.

Plotting the n values as a function of m values for Facies-2 is characterized by relatively high multiplication and exponent values in comparison to the dolomitic facies. This can be attributed to relatively wider pore throats which can be explained by low percentage of micropore spaces where their contribution to permeability is 43.1% (Table 5, Fig. 17). The relatively high petrophysical potential of the siliceous facies is accompanied with weak water wet to neutral wettability (Table 6). Furthermore, this can be explained by the presence of more than 25% macropore spaces and mostly less than 25% micropores; therefore, the required threshold pressure is relatively very low (12.2 psi). These very good petrophysical properties are contributed to good reservoir potential (rank III, Table 7) which forms the main FU1 of Hammam Faraun member and the super conductive zone of FU3 in the topmost parts of Sidri member.

Petrographically, the samples of the petrophysical Facies-3 are described as a dolomitic sublithic arenite microfacies with their arenite and lithic components cemented together by dolomitic material (up to 26% of the total rock), i.e. the pore spaces are completely lined with dolomitic cement and the rock will behave like a dolostone rock. The effect of dolomitization (whether it is porosity-enhancing or porosity-reducing effect) on the petrophysical properties depend mostly on its dominant acting stage. Therefore, the present facies with its 26% dolomitic content is considered to be affected by dolomitization in its middle selective stage which, in turn, means that it is considered as a porosity-enhancing process. However, the presence of some ferruginated clay patches slightly decreased this effect and gives rise to more micropores and nanopores (average micropores = 28.9%, Table 7) than that of the siliceous quartz arenite facies (average micropores = 22.0%, Table 7) as mentioned from the pore throat distribution. In addition, sometimes, the dolomite rhombs are accumulated through the pore throats to increase the percentage of the micropores and to block the pore throats (Fig. 3f). This may be explained by that the dolomitization process is in a transitional stage between the middle and the last stage of dolomitization. Therefore, petrophysically, it is characterized by fair to good

porosity (av. $\varnothing_{He}$ = 12.7) and reasonably by good permeability (av. k_H = 43.3 and av. k_V = 30.6 md, Table 3). Measuring the gas and liquid permeabilites indicates that an average 54.1% of the measured gas permeability is attributed to the presence of micropores that are not accessible to water flow (Fig. 17, Table 5).

The petrophysical properties (porosity and permeability) and behaviour of samples of the dolomitic Facies-3 represent a transitional stage (Figs. 5, 6 and 7) between the petrophysical properties and quality between the argillaceous Facies-1 and the siliceous Facies-2. Since porosity and permeability values of Facies-3 are in a midway between the other two facies, therefore their RQI and FZI average values are also in a midway between the other two petrophysical facies which is mostly related to k values (Fig. 9) and to some extent to $\varnothing_{He}$ and σ_b values (Fig. 8a, b).

In similar to the argillaceous facies, the 'FZI-k_H' relationship of the dolomitic facies shows a high scattering (Fig. 9), which may be attributed to a long diagenetic history of different effects on the studied samples. Plotting the RQI as a function of the FZI ensures the transitional reservoir quality of the dolomitic facies (poor to fair FZI and fair to impervious RQI, Fig. 11a). It is mostly represented by the lower two flow units of Sidri member (FU4, FU6).

From the special core analyses, it is indicated that values of the lithology factor a of the 'FR-∅' relationship of the dolomitic Facies-3 at the ambient and confining pressures are relatively much higher ($a \geq 2.47$) than that for the siliceous facies ($a \leq 1.43$, Table 4). This was attributed by Nabawy (2015) to the carbonate (dolomitic) composition of the studied samples. Similar to the samples of the siliceous Facies-2, values of the lithology factor a increase with increasing the applied pressure which ensures that values of a depend mostly on both the pore fabrics and the petrofabrics where both are affected by increasing pressure.

Concerning the effect of increasing the confining pressure on PR of the present facies (PR $\leq$ 9.76%, Table 5) is less intensive than that of the siliceous facies, which may be attributed to its hard resistant dolomitic composition. In addition, the multiplication factor for the relationship is relatively low ($\leq$21.5, Fig. 13b), which is an additional indication for the dolomitic nature.

Most of the studied plugs show strong to weak oil wet (Table 6, Fig. 18), which can be attributed to the dolomitic nature of that plugs where the carbonate (dolomitic) rocks are mostly oil wet due to the mutual relation between the mineral oil and the surface of the dolomite rhombs.

Since the dolomitic facies is characterized by transitional petrophysical properties between the studied argillaceous and siliceous facies, therefore its quality varies between rank III and rank IV (Fig. 19a, b, Table 7) but shifts in average to rank IV. This can be attributed to the pore throat distribution of this petrophysical facies, where more than 25% of the pore spaces

are in the range of micropores and less than 25% pore spaces are in the range of macropores (Table 7).

Therefore, the present study stated that each petrophysical facies is characterized by a diagnostic set of average petrophysical parameters and relationships. The high reliability of the obtained X-Y plots indicates that discriminating the studied samples, based on their mineral composition integrated with their pore fabrics and petrofabrics, into different petrophysical facies and flow units is a useful tool for evaluating the potential of the given reservoir sequence.

Conclusions

Petrophysically and petrographically, the studied Belayim sandstone sequence can be discriminated into three facies: (1) Facies-1 (composed of argillaceous subfeldspathic arenite microfacies), (2) Facies-2 (composed of siliceous quartz arenite microfacies) and (3) Facies-3 (composed of dolomitic sublithic arenite microfacies). Each microfacies is characterized by its petrophysical properties and behaviour due to its cementation material which lines and coats the pore spaces and channels.

Grain density of the dolomitic Facies-3 is the highest (due to its dolomitic content), whereas that of the argillaceous Facies-1 is the lowest (due to its argillaceous content). Cementation by the argillaceous and the dolomitic materials and their accumulation in the pore throats reduced the reservoir properties of these two facies to lower grades. On the other side, fracturing, dissolution and leaching out are the most porosity-enhancing factors. A set of X-Y plots and empirical equations of high reliability has been introduced for the different petrophysical facies. Each facies has its diagnostic petrophysical parameters and empirical equations which can be used to differentiate their samples from the other samples and to calculate one parameter in terms of another.

Petrophysically, porosity depends mostly on the bulk density, and it is the main contributor to the permeability which, in turn, controls the RQI of the studied facies.

Based on the petrophysical values, the pore throat distribution and the plot of the 'RQI-FZI', it is achieved that the siliceous Facies-2 (the main composition of Hammam Faraun member and the top of Sidri member) has the best reservoir properties (rank III, macropores ≥25% and micropore and nanopores <25%), and the argillaceous Facies-1 (which constitutes many parts of Sidri member) has the worst petrophysical properties (rank VI, 0% macropores and ≥50% micropores and nanopores), whereas the dolomitic Facies-3 (which forms many parts of Sidri member) shows a transitional petrophysical properties between both facies.

Finally, most of the studied rock samples are oil wet with few exceptions for the siliceous facies (sometimes are neutral to water wet). The Belayim sequence can be discriminated vertically into six flow units (FU1–FU6); three of them (FU1, FU3 and FU5) have good reservoir potential and are alternated with the other three units which have bad reservoir properties (FU2, FU4 and FU6).

Therefore, integration between the petrographical, conventional and special core analyses is a useful tool for conducting a precise formation evaluation by discriminating the studied reservoir into flow units and facies.

References

Al-Dhafeeri AM, Nasr-El-Din HA (2007) Characteristics of high permeability zones using core analysis, and production logging data. J Petrol Sci and Eng 55:18–36

AlSharhan AS, Salah MG (1994) Geology and hydrocarbon habitat in a rift setting: southern Gulf of Suez, Egypt

Amaefule JO, Altunbay M, Tiab D, Kersey DG, Keelan DK (1993) Enhanced reservoir description: using core and log data to identify hydraulic (flow) units and predict permeability in uncored intervals/wells. SPE 26436. Presented at the Annual Technical Conference and Exhibition, Houston, TX, pp 3–6

Archie GE (1942) The electric resistivity logs as an aid in determining some reservoir characteristics. Trans Am Int Mech Eng 146:54–62

Bosworth W, Crevello P, Winn RD Jr, Steinmetz J (1998) Structure, sedimentation, and basin dynamics during rifting of the Gulf of Suez and northwestern Red Sea. In: Purser BH, Bosence DWJ (eds) Sedimentation and tectonics of rift basins: Red Sea-Gulf of Aden. Chapman and Hall, London, pp. 77–96

Choquette PW, Pray LC (1970) Geologic nomenclature and classification of porosity in sedimentary carbonates. AAPG Bull 54:207–220

Darwish M, El-Araby AM (1993) Petrography and diagenetic aspects of some siliciclastic hydrocarbon reservoirs in relation to the rifting of the Gulf of Suez. Egypt J Geol 3:1–25

EGPC 'Egyptian Geological Petroleum Corporation' (1964) Miocene rock stratigraphy of the Gulf of Suez, Egypt. Internal Report p 412. Cairo

El Sharawy MS, Nabawy BS (2016) Geological and petrophysical characterization of the Lower Senonian Matulla Formation in Southern and Central Gulf of Suez, Egypt. Arab J Sci Eng 41(1):281–300

El-Gezeery MV, Marzouk IM (1974) Miocene rock stratigraphy of Egypt. J Egypt Geol Soc 18(1):1–59

El-Khadragy AA, Eysa EA, Khedr FI, Saleh AH (2016) Reservoir characteristics of Belayim Formation in Belayim land oil field, Southwest Sinai, Egypt, using core and well logging analysis. International Journal of Scientific Engineering and Applied Science (IJSEAS) 2(1):435–450

Gawad WA, Gaafar I, Sabour AA (1986) Miocene stratigraphic nomenclature in the Gulf of Suez region. In: Egyptian General Petroleum Corporation, 8th Exploration Conference, pp 1–20

Hughes GW, Abdine S, Girgis MH (1992) Miocene biofacies development and geological history of the Gulf of Suez, Egypt. Mar Pet Geol 9:2–28

Jarrige JJ, Ott d'Estevou P, Burollet PF, Montenat C, Richert JP, Thiriet JP (1990) The multistage tectonic evolution of the Gulf of Suez and northern Red Sea continental rift from field observations. Tectonics 9:441–465

Kassab MA, Teama MA, Cheadle BA, El-Din ES, Mohamed IF, Mesbah MA (2015) Reservoir characterization of the Lower Abu Madi Formation using core analysis data: El-Wastani gas field. Egypt J Afr Earth Sci 110:116–130

Levorsen AI (1967) Geology of Petroleum. W.H. Freeman Company, San Francisco, USA

Meshref WM, Abu Karamat MS, Gindi M (1988) Exploration concepts for oil in the Gulf of Suez. In: 9th Petroleum Exploration and Production Conference, Cairo, 1–24

Montenat C, Ott d'Estevou P, Jarrige JJ, Richert JP (1998) Rift development in the Gulf of Suez and the north-western Red Sea: structural aspects and related sedimentary processes. In: Purser BH, Bosence DWJ (eds) Sedimentation and tectonics of rift basins: Red Sea-Gulf of Aden. Chapman and Hall, London, pp. 97–116

Nabawy BS (2015) Impacts of the pore- and petro-fabrics on porosity exponent and lithology factor of Archie's equation for carbonate rocks. J Afr Earth Sci 108:101–114

Nabawy BS, El Sharawy MS (2015) Hydrocarbon potential, structural setting and depositional environments of Hammam Faraun Member of the Belayim Formation, Southern Gulf of Suez, Egypt. J Afr Earth Sci 112:93–110

Nabawy BS, El-Hariri TY (2008) Electric fabric of subsurface Cretaceous rocks, Abu Gharadig Basin, Western Desert Egypt. J Afr Earth Sci 52(1–2):55–61

Nabawy BS, Géraud Y, Rochette P, Nicolas B (2009a) Pore-throat characterization in highly porous and permeable sandstones. AAPG Bull 93(6):719–739

Nabawy BS, Rochette P, Géraud Y (2009b) Petrophysical and magnetic pore network anisotropy of some cretaceous sandstone from Tushka Basin, Egypt. Geophys J Int 177(1):43–61

Othman A, Nabawy BS, Abdel Hafeez T, Saher M, Abdel KR (2008) Reservoir quality discrimination of the lower part of Bahariya Formation, N. Qarun Oil Field, W.D. Egypt. EGS J 6(1):81–101

Pettijohn FJ, Potter PE, Siever R (1972) Sand and sandstone. Chapter 4, Petrographic Classification and Glossary, pp. 149–174, Springer, New York.

Ramadan FS, Eysa EA (2012) Diagenesis and petrophysical properties of the Middle Miocene (Belayim Formation) at Belayim Land Oil Field, West Sinai, Egypt. Aust J Basic Appl Sci 6(6):309–322

Ramzy M, Steer B, Abu-Shadi F, Schlorholtz M, Mika J, Dolson J, Zinger M (1996) Gulf of Suez basin sequence models e part B. Miocene sequence stratigraphy and exploration significance in the central and the southern Gulf of Suez. In: EGPC 13th Exploration Conference, Cairo, Egypt, vol. 2, pp 242–256

Rashed A (1990) The main fault trends in the Gulf of Suez and their role in oil entrapment. In: 10th Petroleum Exploration and Production Conference, Cairo, pp 1–24

Scott RW, Govean FM (1985) Early depositional history of a rift basin: Miocene in the western Sinai. Palaeogeogr Palaeoclimatol Palaeoecol 52:143–158

Serra O (1988) Fundamentals of well-log interpretation: the acquisition of logging data, Chapter 1, pp. 1–24, 3rd edn. Elsevier, Amsterdam

Tiab D, Donaldson EC (1996) Petrophysics, theory and practice of measuring reservoir rock and fluid transport properties. Gulf Publ. Co., Houston, pp 205–220